

## Jet directions in Seyfert galaxies

A. L. Kinney<sup>1,2,5</sup>, H.R.Schmitt<sup>1</sup>, C.J.Clarke<sup>2</sup>, J.E. Pringle<sup>2,1</sup>, J.S. Ulvestad<sup>3</sup> and R.R.J. Antonucci<sup>4</sup>

### ABSTRACT

Here we present the study of the relative angle between the accretion disk (or radio jet) and the galaxy disk for a sample of Seyfert galaxies selected from a mostly isotropic property, the  $60\mu\text{m}$  flux, and warm infrared colors. We used VLA A-array  $3.6\text{cm}$  continuum data and ground based optical imaging, homogeneously observed and reduced to minimize selection effects. For parts of the analysis we enlarged the sample by including galaxies serendipitously selected from the literature. For each galaxy we have a pair of points  $(i, \delta)$ , which are the inclination of the galaxy relative to the line of sight and the angle between the jet projected into the plane of the sky and the host galaxy major axis, respectively. For some galaxies we also had information about which side of the minor axis is closer to Earth. This data is combined with a statistical technique, developed by us, to determine the distribution of  $\beta$  angles *in 3 dimensions*, the angle between the jet and the host galaxy plane axis.

We found from an initial analysis of the data of the  $60\mu\text{m}$  sample, where Seyfert 1's and 2's were not differentiated, that the observed distribution of  $i$  and  $\delta$  values can be well represented either by a homogeneous  $\sin\beta$  distribution in the range  $0^\circ \leq \beta \leq 90^\circ$ , or  $0^\circ \leq \beta \leq 65^\circ$ , but not by an equatorial ring. A more general model, which tested  $\beta$ -distributions in the range  $\beta_1 \leq \beta \leq \beta_2$ , for different ranges of  $\beta_1$  and  $\beta_2$  values, required  $\beta_2$  to be larger than  $65^\circ$  and gave preference for  $\beta_1$  smaller than  $40^\circ - 50^\circ$ . An important result from our analysis was obtained when we distinguished if the jet was projected against the near or the far side of the galaxy, and differentiated between Seyfert 1's and Seyfert 2's, which showed that the model could not represent Seyfert 1's adequately. We found that the inclusion of viewing angle restrictions for Seyfert 1's, namely, that a galaxy can only be recognized as a Seyfert 1 if the angle between the jet and the line of sight ( $|\phi|$ ) is smaller than a given angle  $\phi_c$  and that the galaxy

---

<sup>1</sup>Space Telescope Science Institute, 3700, San Martin Drive, Baltimore, MD 21818, USA

<sup>2</sup>Institute of Astronomy, The Observatories, Madingley Road, Cambridge CB3 0HA, England.

<sup>3</sup>National Radio Astronomy Observatory, P.I. Box O, 1003 Lopezville Road, Socorro, NM, 87801, USA

<sup>4</sup>University of California, Santa Barbara, Physics Department, Santa Barbara, CA 93106, USA

<sup>5</sup>Present address: NASA Headquarters, 300 E St., Washington, DC20546

inclination  $i$  is smaller than an angle  $i_c$ , gave rise to statistically acceptable models. This indication that there is a difference in viewing angle to the central engine between Seyfert 1's and Seyfert 2's is a direct and independent confirmation of the underlying concepts of the Unified Model.

We discuss possible explanations for the misalignment between the accretion disk and the host galaxy disk, which are: warping of the accretion disk by self-irradiation instability, by the Bardeen-Petterson effect, or by a misaligned gravitational potential of a nuclear star cluster surrounding the black hole, as well as feeding of the accretion disk by a misaligned inflow of gas from minor mergers, capture of individual stars or gas from the nuclear star cluster, or the capture of individual molecular clouds from the host galaxy.

*Subject headings:* galaxies:active – galaxies:jets – galaxies:Seyfert – galaxies:structure

## 1. Introduction

We would expect, based on grounds of symmetry and simplicity, that the jets emanating from a Seyfert nucleus would emerge at right angles to the disk of the host spiral galaxy. The processes for bringing material close to the core (within the innermost 10pc) of a galaxy, either for the initial formation of the black hole or to provide fuel to the black hole, are of two sorts – those that feed the nucleus from the visible gas reservoir in the galaxy disk, and those that feed the nucleus by introducing material from outside the galaxy. In the simplest pictures, fueling by both internal gas and by external gas favors co-alignment between accretion disk and galaxy disk, since most of the gas is in the galaxy disk and any gas added to it may rapidly end up there, either by shocks or by settling in the galaxy potential. Since the jets are launched perpendicular to the accretion disk, the simplest assumption would be to see them aligned to the host galaxy minor axis.

However, the above scenario is flatly contradicted by the observations. Investigations of the observed distribution of the angle  $\delta$ , the difference between the position angle of the major axis of the galaxy and the position angle of the radio jet projected on the plane of the sky, shows that Seyfert galaxies can have jets along any direction, from aligned along the minor axis to aligned along the major axis (Ulvestad & Wilson 1984; Brindle et al. 1990; Baum et al. 1993; Schmitt et al. 1997; Nagar & Wilson 1999). It was shown by Clarke, Kinney & Pringle (1998), using data for a sample of Seyfert galaxies selected from the literature, that it is possible to obtain a reliable estimate of the distribution of the angle  $\beta$  *in 3-dimensions* between the jet axis and the normal to the galaxy plane, by considering for each galaxy in the sample, the pair of values of  $i$  and  $\delta$  ( $i$  is the inclination of the galaxy to the line of sight). They conclude that the directions of the radio jets are consistent with being completely uncorrelated with the planes of the host galaxies (see also Nagar & Wilson 1999).

The observed random alignment between accretion disks and galaxy disks is intriguing, and the study of this effect is important for the understanding of the inner workings of Seyfert galaxies. This result may imply, for example, that recently suggested ideas about radiation induced warping of accretion disks (Pringle 1996, 1997, and Maloney, Begelman & Pringle 1996) come into play both to determine the directionality of the accretion disk and to produce the ionization cones, or that the warping is caused by the rapid spinning of the central black hole with spin misaligned with the spin of the galaxy (Bardeen-Petterson effect). Alternatively, this misalignment may result by the feeding of the accretion disk from gas outside the galaxy, by mergers, for example.

Here we study the distribution of angles  $\beta$  in a well defined sample of Seyfert galaxies, selected from a mostly isotropic property, the flux at  $60\mu\text{m}$ , and warm infrared colors (de Grijp et al. 1987, 1992). Most of the previous works in this subject used samples selected from the literature and were likely to suffer from selection effects. The example of one problem possibly caused by selection effects was the “zone of avoidance” found by Schmitt et al. (1997), a region of  $20^\circ$  around the host galaxy minor axis where no jets were detected, but which was shown later by Nagar & Wilson (1999) to be due to the sample. Another problem of previous papers was the use of data collected from the literature, measured by different authors, using different methods, which resulted in uncertainties that cannot be quantified. We have addressed this problem by using radio and optical data observed, reduced and measured in a homogeneous way.

This paper is organized in the following way. In Section 2 we discuss the details about the data and the samples. In Section 3 we present the geometry of the problem and the statistical technique used to determine the distribution of  $\beta$  angles. In Section 4 we compare the data with the models, determine which  $\beta$ -distribution and what kind of restrictions are required to better represent the observed data. In Section 5 we discuss a series of possible explanations for the observed misalignment between the accretion disk and the host galaxy disk, and finally in Section 6 we give a summary of the work.

## 2. The data

### 2.1. The $60\mu\text{m}$ sample

The previous studies on relative angle in different types of Seyfert galaxies (Ulvestad & Wilson 1984; Brindle et al. 1990; Baum et al. 1993; Schmitt et al. 1997; Nagar & Wilson 1999) were not based on well defined samples. Most of these papers used data selected from the literature, and were most likely biased with respect to orientation. One possible bias would be the preferential selection of galaxies which have jets shining into the plane of the galaxy, resulting in brighter radio emission and narrow line regions, which would be easier to detect. Another possible selection effect happens in the case of Seyferts selected by ultraviolet excess. According to the Unified Model, we see  $\approx 1\%$  of the nuclear continuum by reflection in Seyfert 2’s, and the whole continuum in Seyfert 1’s, which means that Seyfert 2’s selected in this way are on the higher

luminosity end of the luminosity function and are likely to have stronger and more extended radio emission. In an attempt to alleviate this problem we are using a sample chosen from a mostly isotropic property, the flux at  $60\mu\text{m}$ . According to the torus models of Pier & Krolik (1992), which are the most anisotropic and hence the most conservative models, the circumnuclear torus radiates nearly isotropically at  $60\mu\text{m}$ .

Our sample includes 88 Seyfert galaxies (29 Seyfert 1's and 59 Seyfert 2's), which correspond to all galaxies from the de Grijp et al. (1987, 1992) sample of warm IRAS galaxies with redshift  $z \leq 0.031$ . The galaxies in this sample were selected based on the quality of the  $60\mu\text{m}$  flux, Galactic latitude  $|b| > 20^\circ$ , and  $25\mu\text{m}$ – $60\mu\text{m}$  color in the range  $-1.5 < \alpha(25/60) < 0$ , chosen as to exclude starburst galaxies as much as possible. The candidate AGN galaxies were all observed spectroscopically (de Grijp et al. 1992) to confirm their activity class as being Seyfert 1 or Seyfert 2 and *not* a lower level of activity such as starburst or LINER. The distance limit of  $z \leq 0.031$  allows us to study a statistically significant number of objects which are nearer, and thus more likely to be resolved in the radio.

We note that although the use of the  $60\mu\text{m}$  sample provides an initial object selection that is expected to be more or less isotropic, the optical follow up required to classify the galaxies spectroscopically inevitably re-introduces a degree of orientation bias. We find however that the objects in the  $60\mu\text{m}$  sample contain a higher proportion of more nearly edge-on galaxies than do objects selected serendipitously from the literature. This provides some *a posteriori* justification for the notion that the orientation bias is *weakened* (though not removed) by use of this sample (see a further discussion in 4.4.4). In any case, a major benefit of the  $60\mu\text{m}$  sample is that its use considerably speeds up the process of weeding out the (very many) galaxies without Seyfert or starburst activity, and assures that Seyfert 1's and Seyfert 2's are matched in luminosity.

In Figure 1 we show the histogram of the  $60\mu\text{m}$  luminosity distribution for the Seyfert 1's and Seyfert 2's in our sample. This demonstrates that the sample has no significant difference in luminosities between the two types, with a KS test showing that there is a 45.3% chance that two samples drawn from the same parent population would differ this much, or more. Similarly, Keel et al. (1994) shows that both the [OIII] and the IR luminosities for the  $60\mu\text{m}$  sample have very similar distributions, demonstrating that selection according to the  $60\mu\text{m}$  flux is unlikely to bias the survey towards either Seyfert 1s or Seyfert 2s. In particular, this histogram shows that we are selecting the subtypes from the same part of the luminosity function.

Of the 88 galaxies in our sample, 77 have  $\delta > -47^\circ$  and can be observed from VLA in a reasonable amount of time. Of these 77 galaxies, 38 were previously observed with the A-array in X-band (3.6cm) and are available in the archive. We carried out a snapshot survey to observe 36 of the remaining 39 galaxies, using the same frequency and configuration (Schmitt et al. 2000). As a result, we have A-array X-band (3.6cm) data, which gives a spatial resolution of  $\approx 0.24''$ , for 74 galaxies. One of these galaxies, TOL1238-3364, was not detected, while for one of the galaxies in the southern hemisphere, PKS2048-57, which cannot be observed from VLA, we got literature

data from Morganti et al. (1999), who observed it with ATCA also at 3.6cm.

We reduced the data for the 36 galaxies in our sample, as well as for 21 of the 38 galaxies available in the archive, for which there was no data previously published, or for which we could find better data in the archive. Details about the reduction of the radio data and a discussion on individual objects can be seen in Schmitt et al. (2000). The 17 remaining objects were obtained from the literature, only using data that were reduced and analyzed in a way similar to ours. The sample is presented in Table 1 where we show the de Grijp et al. (1987) number of the galaxies, their names, activity class, radial velocity,  $60\mu\text{m}$  luminosity, radio 3.6cm flux, 3.6cm luminosity and the extent of the radio emission at 3.6cm.

While 74 out of 75 galaxies observed at 3.6cm were detected, 36 of these objects,  $\approx 50\%$  of the sample, show extended emission. For those objects with linear extent (based on the Ulvestad and Wilson 1984 definition), the radio emission was decomposed into individual components by fitting Gaussians to them. The radio position angle ( $\text{PA}_{\text{RAD}}$ ) is measured between the central position of these Gaussians. We estimate that the error in the measurements is of the order of  $3^\circ - 5^\circ$  for linear extended radio sources and  $5^\circ - 10^\circ$  for slightly resolved radio sources. For MCG-03-34-064 we measured  $\text{PA}_{\text{RAD}}$  using only the inner  $0.5''$  of the jet, because outside this region the jet changes direction, bending to the south. For MRK348, NGC1068 and NGC5506, instead of using the VLA data we used higher resolution VLBA data from Ulvestad et al. (1999), MERLIN data from Gallimore, Baum & O’Dea (1996) and VLBA data from Roy et al. (2000), respectively. This data gives the orientation of the jet closer to the nucleus, which in some cases is different from the orientation seen on VLA scales. We note that in the case of NGC1068 we used  $\text{PA}_{\text{RAD}} = 0^\circ$ , since the inner E-W radio structure is related to the torus (Gallimore et al. 1996).

We estimate that the influence of galaxy disk emission is not important in the determination of the position angle of extended radio emission in the more distant galaxies of our sample. The emission from the galaxy disk is usually diffuse and weak, and largely resolved out in our high resolution observations: most of our galaxies just show small linear extended emission in the nucleus. There is the possibility that part of the extended emission in slightly extended sources could be due to circumnuclear star formation. However, since the extended emission was usually detected on scales smaller than  $1'' - 2''$ , and the spectra used to classify these galaxies were obtained with a similar aperture, these galaxies would probably have been classified as Starbursts.

Another limitation of previous papers on the orientation of radio jets relative to the host galaxy in Seyferts was the use of inhomogeneous information about the position angle of the major axis, and inclination of the galaxy ( $\text{PA}_{\text{MA}}$  and  $i$  hereafter). Most of these studies used data from the literature, or measured the values from the Digitized Sky Survey I, which does not have good enough resolution for sources smaller than  $\approx 1'$ . To solve this problem we obtained high signal to noise ratio ground based B and I images for almost all the galaxies in the sample (for a small number of galaxies it was possible to observe only one of the bands). The data were taken at CTIO, KPNO and Lick Observatory. The reduction and analysis are reported in detail by Schmitt

& Kinney (2000).

The values of  $PA_{MA}$  and the inclination were obtained by fitting ellipses to the images of the galaxies. The values of  $PA_{MA}$  were measured directly from the ellipses fitted to the isophotes corresponding to the surface brightness level 24-25 B mag arcsec<sup>-2</sup>. We point out that this level is usually deep enough to avoid the problem of bars and oval distortions, besides the fact that we have also checked the images of the galaxies for these effects. Assuming that the galaxies are circular when seen face-on, we can use the ellipticity of the outer isophotes to determine their inclinations  $i$ . To do this we used the relation  $\cos i = b/a$ . We compared the values obtained using this method with the values obtained using the empirical formula  $\sin^2 i = [1 - (b/a)^2]/0.96$  from Hubble (1926), which takes into account the thickness of the galaxy disk. Since the difference between the two measurements was always smaller than 1° to 2°, which is less than or approximately of the order of the measurement errors, we decided to use the values obtained using the first relation. We estimate that the error in the determination of the host galaxy inclination and  $PA_{MA}$  is of the order of 2° – 4° for the more inclined galaxies, and larger for the face-on galaxies, where it can be as much as 6°. For a small number of galaxies it was possible to find values of  $PA_{MA}$  and  $i$  obtained from kinematical data in the literature. Since this is the most precise way to determine these quantities, whenever it was possible we used these measurements instead of ours.

In this paper we introduce an important improvement relative to previous studies, which is the use of information about which side of the minor axis of the galaxy is closer to Earth. As pointed out by Clarke et al. (1998), this information can improve the statistics of the sample by a factor of two, because we constrain the jet to lie along a particular segment of the great circle. One way we used to obtain this information was the inspection of dust lanes in the images of the galaxies. We expect to see dust lanes only in the closer side of the galaxy, since they are highlighted against background bulge light. A considerable number of objects show dust lanes, either in our B and I images, or higher resolution HST V band images.

For galaxies where it was not possible to detect dust lanes, we obtained the information about the galaxy orientation from the rotation curve of the galaxy and the direction of the spiral arms. Assuming that the spiral arms are trailing and knowing which side of the galaxy is approaching Earth, we can determine which side of the minor axis is closer. To do this we used rotation curves from the literature and also obtained, for several galaxies in the sample, long-slit spectra aligned close to the major axis. Our spectra were obtained at CTIO and La Palma observatory and will be published elsewhere. We were able to obtain the information about the closer side of the minor axis for approximately two thirds of the sample with extended radio emission. Most of the objects for which we were not able to obtain this information were S0 galaxies, for which we could not see the spiral arms and also do not show dust lanes, or galaxies very close to face-on, where it is difficult to obtain a reliable rotation curve.

In Table 2 we show the 36 galaxies with extended radio emission, their activity classes,  $PA_{MA}$ ,  $i$ ,  $PA_{RAD}$ , the side of the galaxy closer to Earth and the morphology of the extended radio

emission, according to the Ulvestad & Wilson (1984) method. Notice that NGC5548, MRK176 and NGC7212 are being shown in this Table just for completeness, because they are interacting galaxies and will not be used in the analysis.

## 2.2. Serendipitous sample

In some sections of the paper we will also use a larger sample, consisting of 69 galaxies, all Seyferts known to have extended radio emission. This sample is composed of 33 galaxies from the  $60\mu\text{m}$  sample, plus 36 additional galaxies serendipitously obtained from the literature (e.g. Schmitt et al. 1997, Nagar & Wilson 1999). We point out that, for most of the 36 serendipitous galaxies, the values of  $\text{PA}_{\text{RAD}}$ ,  $\text{PA}_{\text{MA}}$  and  $i$  were obtained from the literature. For some of these galaxies,  $\text{PA}_{\text{RAD}}$  was obtained from Nagar et al. (1999), so they were measured in a way similar to that of the  $60\mu\text{m}$  sample. Also, we were able to obtain B and I images for some of these galaxies (Schmitt et al. 2000), which insures homogeneous measurements of  $\text{PA}_{\text{MA}}$  and  $i$ . However, most of the measurements for these 36 galaxies come from inhomogeneous datasets, done using different methods. In Table 3 we show the 36 galaxies from the serendipitous sample, their activity classes,  $\text{PA}_{\text{MA}}$ ,  $i$ ,  $\text{PA}_{\text{RAD}}$ , the side of the galaxy closer to Earth and the morphology of the extended radio emission.

## 3. Statistical Analysis

### 3.1. Geometry

The geometry of our analysis has been described by Clarke, Kinney & Pringle (1998), but is repeated here for completeness. For each galaxy we can determine two observational parameters,  $i$  and  $\delta$ . The angle  $i$  is the inclination of the plane of the galaxy to the plane of the sky, or equivalently the angle between the line of sight and the vector normal to the galaxy plane. The angle  $i$  lies in the range  $0^\circ < i < 90^\circ$ . We use a Cartesian coordinate system OXYZ (see Figure 2) so that OX lies along the apparent major axis of the galaxy disk, OY lies along the apparent minor axis, and thus OZ is the vector normal to the galaxy plane. In these coordinates the unit vector in the direction of the line of sight is

$$\mathbf{k}_s = (0, -\sin i, \cos i). \quad (1)$$

The angle  $\delta$  corresponds to the difference between the position angle of the apparent major axis of the galaxy and the position angle of the radio jet projected onto the plane of the sky. By convention  $\delta$  is taken to lie in the range  $0^\circ < \delta < 90^\circ$ . The definition of all the angles involved in the geometry of the problem, the angles used in the models, and their allowed values is given in Table 4.

For a given value of  $\delta$  and  $i$ , the direction of the jet, which we denote by a unit vector  $\mathbf{k}_j$  is determined to lie on a great circle drawn on a unit sphere centered at the origin of our coordinate system. In the OXYZ coordinates described above the great circle is the set of points:

$$\mathbf{k}_j = (k_{jx}, k_{jy}, k_{jz}) = (\cos \delta \sin \phi, \sin \delta \cos i \sin \phi - \sin i \cos \phi, \sin \delta \sin i \sin \phi + \cos i \cos \phi), \quad (2)$$

where  $\phi$  is the angle between the vectors  $\mathbf{k}_s$  and  $\mathbf{k}_j$  between the jet and the line of sight, and formally lies in the range  $-180^\circ < \phi < 180^\circ$ . We should also note that there is a mirror symmetry to the problem about the apparent minor axis of the galaxy, that is about the OYZ plane. In terms of our coordinates this translates into the statement that reversing the direction of the OX axis leaves the problem unchanged. Thus, formally, the sign of  $k_{jx}$  is not an observationally meaningful quantity, or in other words the jet vector in fact lies on one of two great circles which are reflections of each other in the OYZ plane. We have therefore simplified the discussion by considering just one of these great circles.

If we define  $\beta$  as the angle the jet vector  $\mathbf{k}_j$  makes with the disk normal OZ, then we see from Equation 2 that

$$\cos \beta = k_{jz} = \sin \delta \sin i \sin \phi + \cos i \cos \phi. \quad (3)$$

Then the only relevant values of  $\phi$  are those which give  $0^\circ < \beta < 90^\circ$ , or  $\cos \beta > 0$ . In terms of  $\phi$ , this means that  $\phi$  lies in the range  $\phi_1 < \phi < \phi_1 + 180^\circ$ , where  $\phi_1 (< 0)$  is the value of

$$\phi_1 = \tan^{-1}(-\cot i / \sin \delta), \quad (4)$$

which lies in the range  $-90^\circ < \phi_1 < 0^\circ$ . We note that physically, if  $\phi < 0$ , then the jet vector is projected against the half of the galaxy disk which is nearest to us, whereas  $\phi > 0$  corresponds to the jet being projected against the half of the galaxy disk which is furthest from us.

What we are trying to determine is the distribution of the directions of the jets, relative to their host galaxies ( $\beta$ ). Relative to the host galaxy we will assume that the jet direction is given by the unit vector  $\mathbf{k}_j$  where,

$$\mathbf{k}_j = (\sin \beta \cos \theta, \sin \beta \sin \theta, \cos \beta). \quad (5)$$

Thus the jet direction is determined by the two angles  $\beta$  and  $\theta$ , where  $\beta$  is the angle the jet axis makes with the symmetry axis of the galaxy, and  $\theta$  is the azimuthal angle about that axis.

### 3.2. Estimation of the $P(\beta)$ distribution

The value of the azimuthal angle  $\theta$  for a particular galaxy is not an intrinsic property of the galaxy but just depends on the orientation of the galaxy relative to the line of sight. In contrast the angle  $\beta$  is an intrinsic property of the galaxy and is the angle we would like to be able to determine. In fact what we would like to determine is the distribution of angles  $\beta$  the jet vectors

in our sample make with the galaxy normal. We denote this distribution in terms of a probability distribution  $P(\beta)$ , which is defined so that

$$\int_0^{\pi/2} P(\beta) d\beta = 1. \quad (6)$$

Thus, for example, if the jet axes were randomly oriented in space, and thus were independent of the galaxy disc, then we would find that  $P(\beta) = \sin \beta$ .

In order to proceed with our analysis, we shall initially make two assumptions. First, we assume that all values of  $\theta$  are equally likely to occur in nature. This is reasonable, since otherwise we would have some special place in the Universe. Second, we assume that the inclusion of a galaxy in our sample is independent of the value of  $\theta$ . This is a more problematic assumption, and we return to it below in our discussion of selection effects (Section 4.4).

Since, as will become apparent, we do not have enough data points to determine  $P(\beta)$  directly (even if our sample were not subject to selection effects), we shall adopt the procedure of taking model distributions of  $P(\beta)$  and asking if, in a statistical sense, they are consistent with the data. The trial distributions we shall consider correspond to the jet directions, as seen from the nucleus of the host galaxy, being randomly distributed over a band on the sky given by  $\beta_1 \leq \beta \leq \beta_2$ , and we shall denote these distributions as  $P(\beta | \beta_1, \beta_2)$ . As we shall see in Section 4 these model distributions are sufficiently general, given the data we are dealing with.

### 3.2.1. Estimation of $P(\beta)$ at a fixed value of $i$

It is simplest to understand the procedure for estimating  $P(\beta)$  from the observed distribution of  $\delta$ , if we initially consider the procedure at a fixed value of the galaxy inclination  $i$ . We shall suppose therefore that we have a set of  $N$  galaxies, each observed at the same value of  $i$ , and that for each galaxy  $k$ , for  $1 \leq k \leq N$ , there is an observed value of  $\delta$ ,  $\delta_k$ , such that  $0^\circ \leq \delta_k \leq 90^\circ$ . As discussed above, for a galaxy at a given value of  $i$ , the observation of the value of  $\delta$  implies that the unit vector  $\mathbf{k}_j$  lies along a great circle given by Equation 2. Thus at a given value of  $i$ , the probability distribution  $P(\beta)$  for  $\beta$  implies a corresponding probability distribution  $P(\delta | i)$  for  $\delta$ . For example, if  $\beta_1 = 0^\circ$ , and  $\beta_2 = 90^\circ$ , so that the jet directions are randomly oriented over the whole sky, then  $P(\delta)$  would be a constant, independent of  $\delta$ , because then all great circles would be equally likely. Thus if we had a large sample of galaxies all at the same inclination  $i$ , we could test the hypothesis that the jet directions were uniformly distributed over the sky, simply by testing the observed  $\delta$  distribution to see if it was uniformly distributed in the allowed range  $0^\circ \leq \delta \leq 90^\circ$ .

More generally, if the jet directions are uniformly distributed over the band on the sky  $\beta_1 \leq \beta \leq \beta_2$ , then the distribution for  $\delta$ , at given  $i$  is given by  $P(\delta | i, \beta_1, \beta_2)$ , where  $\delta$  is distributed

over the range  $\delta_{\min} \leq \delta \leq 90^\circ$ , and

$$\int_{\delta_{\min}}^{\pi/2} P(\delta | i, \beta_1, \beta_2) d\delta = 1. \quad (7)$$

The expressions for  $P(\delta | i, \beta_1, \beta_2)$  are given in Appendix A.

We note that the lower end of the possible range for  $\delta$  is not necessarily zero. This is because the circle  $\beta = i$  and the great circle defined by  $\delta = 0$  touch at the line of sight vector  $\mathbf{k}_s$ . Thus if  $\beta_2 < i$ , there is a range of values of  $\delta$ ,  $0 \leq \delta \leq \delta_{\min}$  such that the great circles do not intersect the polar region  $\beta \leq \beta_2$ .

All points on a given great circle, defined by  $(i, \delta)$ , lie at values of  $\beta \geq \beta_{\min}(i, \delta)$ , where

$$\begin{aligned} \beta_{\min}(i, \delta) &= \cos^{-1}(\sin^2 \delta \sin^2 i + \cos^2 i)^{1/2}, \\ &= \sin^{-1}(\sin i \cos \delta) \end{aligned} \quad (8)$$

(Clarke, Kinney & Pringle, 1998). Thus if  $\beta_2 < i$ , then the minimum value  $\beta$  can take is such that  $\beta_{\min} = \beta_2$ . Thus, using equation 8 we find that:

$$\begin{aligned} \delta_{\min} &= 0 && (\beta_2 > i) \\ &= \cos^{-1}(\sin \beta_2 / \sin i) && (\beta_2 < i). \end{aligned} \quad (9)$$

Thus, if we had a sample of  $N$  galaxies, all observed at the same inclination  $i$ , to check the consistency of the data with the model distribution  $P(\beta | \beta_1, \beta_2)$ , the procedure to follow would be to compare the observed distribution of values of  $\delta$  with the distribution predicted by the model, by means of some suitable statistical test. The test we shall use is one which is straightforwardly generalizable to more complicated datasets, and the procedure is as follows. In general, the distribution  $P(\delta | i, \beta_1, \beta_2)$ , which we derived from our model distribution  $P(\beta | \beta_1, \beta_2)$  is not uniform. For each datapoint  $\delta_k$ , for  $1 \leq k \leq N$ , the centile point  $c_k$ ,  $0 \leq c_k \leq 1$  is defined such that:

$$c_k = \int_{\delta_{\min}}^{\delta_k} P(\delta | i, \beta_1, \beta_2) d\delta. \quad (10)$$

Then, of course, the values,  $c_k$ ,  $1 \leq k \leq N$  should be uniformly distributed on the interval  $[0, 1]$ . We then use the KS test to see with what degree of confidence the  $c_k$  distribution is consistent with being drawn from a uniform distribution.

### 3.2.2. Estimation of $P(\beta)$ for a general dataset

In general, of course, for the actual dataset of  $N$  galaxies in the sample, each galaxy is not observed at the same inclination  $i$ . Thus for each galaxy,  $k$ , in the sample, for  $1 \leq k \leq N$ , we have the observed pair of values  $(i_k, \delta_k)$ . Thus for each datapoint, for a given assumed model for the  $\beta$ -distribution,  $P(\beta | \beta_1, \beta_2)$ , there is a corresponding  $\delta$ -distribution,  $P(\delta | i_k, \beta_1, \beta_2)$ . It is

now, however, straightforward to generalize the statistical procedure discussed above. For each datapoint  $k$ , we define the centile,  $c_k$ , such that

$$c_k = \int_{\delta_{\min}}^{\delta_k} P(\delta | i_k, \beta_1, \beta_2) d\delta. \quad (11)$$

Then it is still true, even for this more general dataset, that if the galaxy sample is indeed chosen from a set of galaxies with distribution  $P(\beta | \beta_1, \beta_2)$ , then the values  $c_k$ , for  $1 \leq k \leq N$  should be uniformly distributed in the interval  $[0, 1]$ . As before, we may use the KS test to ascertain the likelihood of this hypothesis.

### 3.2.3. Introduction of additional constraints

The utility of the statistical procedure we have adopted becomes apparent as soon as we need to add additional information to the data, and/or additional constraints to the models. For example, for some of the galaxies in our sample we have the additional information as to whether the jet is seen in projection against the near side or far side of the galaxy. If we are prepared to make the additional assumption that the observed jet (or the stronger of the two in the case of a two-sided jet) is the one that lies above the host galaxy plane (as seen from Earth), then for a given pair of values of  $(i, \delta)$ , the arc of the great circle on which the end of the jet can lie, is further constrained (Section 3.1). In addition we may wish to add to our set of models, against which the data is being tested, some aspects of the unified model, such as restrictions on  $\phi$  the angle between the jet axis and the line of sight, depending on whether the AGN is a Seyfert 1 or a Seyfert 2.

Whatever additional assumptions we wish to impose on interpretation of the data and/or on the models to be tested, it is evident that for each galaxy,  $k$ , in the sample at its given value of  $i_k$  we can calculate, given the additional assumptions/constraints, a distribution in  $\delta$ . From that distribution in  $\delta$ , and the value of  $\delta_k$  for that galaxy, we can calculate the centile,  $c_k$ . Note that since the centiles,  $c_k$  are computed on a galaxy by galaxy basis, we do not need to have the same type of information available for each galaxy. If the data are consistent with the model, then the values  $c_k$  should still be distributed uniformly in the interval  $[0, 1]$ , and as before we may use the KS test to ascertain the likelihood of our hypotheses.

## 4. Results

In Figure 3 we plot the data in the  $(i, \delta)$  plane. In Figure 3a we plot the total sample (i.e the  $60\mu\text{m}$  sample plus the serendipitous sources) which comprises 69 objects, and in Figure 3b we plot the  $60\mu\text{m}$  sample alone (33 objects). In each Figure we distinguish between the Seyfert 1s and the Seyfert 2s.

As can be seen from the Figures, the distribution of galaxies with inclination shows an apparent dearth of galaxies at low inclinations (face-on) and at high inclinations (edge-on). The

dearth at low inclinations could be a problem for our analysis, since we measure the inclinations by assuming that the outer parts of the galaxies are intrinsically circular. If this were not so, then there would be a systematic upward bias in our inclination determinations. However, if galaxies are oriented randomly in space, then the number density of galaxies is proportional to  $\sin i di$ . If this is taken into account the apparent dearth of low inclination galaxies is consistent with random galaxy orientations (Schmitt et al. 2000). In fact, as far as the analysis of jet orientations is concerned, we learn least from face-on galaxies – the most informative data points are those for galaxies with high inclination (Section 4.1). The dearth of galaxies with high inclination may be due to detectability problems for active nuclei in very edge-on galaxies, but in any case it turns out that the inclination distribution is consistent with those normally found for galaxies in the field (Schmitt et al. 2000). We note that one major advantage of the galaxies from the  $60\mu\text{m}$  sample for our present purposes is that the detection criteria have apparently enabled the identification of a number of AGN with high galaxy inclinations.

In Figure 3a and Figure 3b we also plot contours of constant  $\beta_{\text{min}}$  (Equation 8) in the  $(i, \delta)$ -plane. The value of  $\beta_{\text{min}}$  for each object, derived using Equation 8 from the object’s pair of values  $(i, \delta)$ , is the smallest angle  $\beta$  which the jet in that object can make with the normal to the galaxy plane. In both the total and the  $60\mu\text{m}$  samples, it is evident that the data are incompatible with the jets tending to be closely aligned with the galactic normal. In both samples, at least 40 per cent of the galaxies must have jets lying at greater than  $\beta = 30^\circ$  to the normal, and at least 10 per cent must lie at an angle  $\beta \geq 50^\circ$  (c.f. Clarke, Kinney & Pringle, 1998). The largest value of  $\beta_{\text{min}}$  lies in the range  $60^\circ - 70^\circ$ , so that any model which restricts jets to a circumpolar cap of angular radius less than this is immediately ruled out.

The basic assumptions which underlie all of our analysis of the data are that (i) the set of galaxies in the sky have their jet directions distributed uniformly in azimuth about the normal to the galaxy disk plane *and* (ii) the galaxies in our sample have been randomly selected from that set. While the first of these assumptions is based on the reasonable expectation that galaxies are oriented randomly in space, the second may be more problematic, and we return to it below (Section 4.4). In the meantime we continue with our analysis of the data, gradually introducing more assumptions about the data as we proceed.

#### 4.1. No extra assumptions

We proceed initially without making any extra assumptions. In particular, we shall ignore our knowledge about whether an object is a Seyfert 1 or a Seyfert 2, or equivalently, we shall assume that, in contradiction of the unified model (or related current wisdom), the property of being a Seyfert 1 or a Seyfert 2 is intrinsic to the galaxy, and is independent of the angle from which the nuclear region of that galaxy is viewed.

In order to illustrate how we make use of the distribution of galaxies in  $(i, \delta)$ , we consider

three simple models for the  $\beta$ -distributions, before proceeding to more general models.

*4.1.1. Uniform  $\sin \beta$  distribution:  $\beta_1 = 0^\circ, \beta_2 = 90^\circ$*

If the jets are oriented completely randomly relative to the host galaxies, then, as discussed in Section 3.2.1 we expect the galaxies to be distributed uniformly in  $\delta$  independent of galaxy inclination  $i$ . A visual inspection of Figure 4a and Figure 4b confirms that the distribution of galaxies in  $\delta$  is not strikingly non-uniform in either the  $60\mu\text{m}$  sample, or in the data as a whole. We show the quartiles as lines in Figure 4. Under this uniform  $\sin \beta$  model there should be equal numbers of data points in each quartile marked in the diagram. By inspection it can be seen that this is approximately the case. A more formal analysis, using the KS test, shows that the hypothesis that the data are drawn from a set of galaxies with uniform distribution in  $\sin \beta$  is consistent at the 81% level for the total sample. To be precise, this means that the data, if drawn from the assumed model set of galaxies, would on average differ from the model by the amount observed (or more) 81% of the time. Consistency is at the 67% level for the  $60\mu\text{m}$  sample. Thus in each case, we confirm our visual impression that the distribution of data is consistent with the hypothesis that the jets point randomly with respect to their host galaxies (c.f. Clarke, Kinney, & Pringle, 1998).

*4.1.2. Uniform polecap:  $\beta_1 = 0^\circ, \beta_2 = 65^\circ$*

We now consider a model for the  $\beta$ -distribution of the  $60\mu\text{m}$  data in which the jets are uniformly distributed over a polecap of half angle  $65^\circ$  centered on the normal to the galaxy plane (i.e  $0^\circ \leq \beta \leq 65^\circ$ ). The value of  $65^\circ$  is chosen as being just larger than the largest value of  $\beta_{\text{min}}$  for galaxies in the  $60\mu\text{m}$  sample. It therefore represents the smallest polecap compatible with the  $60\mu\text{m}$  data. As discussed in Section 3.2.1, at each value of  $i$ , an assumed distribution of  $\beta$  gives rise to a corresponding distribution in  $\delta$ . At each  $i$  we may therefore compute the quartiles of the expected  $\delta$ -distribution, and by joining together the quartile points at different values of  $i$  we may plot quartile lines in the  $(i, \delta)$ -plane. In Figure 5 we plot the quartile lines for the  $0^\circ \leq \beta \leq 65^\circ$  polecap model, as well as the  $60\mu\text{m}$  data. If the data are a true sample from the model then we would expect (on average) an equal number of data points to fall within each quartile on the diagram. A KS test indicates that the data are consistent with the model at the 69% level. Thus this mildly aligned model is not ruled out by the data.

We draw attention briefly to the shape of the quartile contours in the  $(i, \delta)$ -plane. At low values of  $i$ , the quartiles tend to those for the randomly oriented jet model. This must be so, because, when the galaxy is viewed face-on, a random distribution of jets in azimuth (assumption (i) above) translates into a uniform distribution in  $\delta$ . For larger values of  $i$ , the quartiles differ significantly from the random jet orientation model, and for this assumed  $\beta$ -distribution they bend

towards higher values of  $\delta$ . For inclinations  $i > 65^\circ$  there is an excluded area (the zeroth centile), since a galaxy with a value of  $(i, \delta)$  in this area would imply a jet with  $\beta_{\min} > 65^\circ$ , and therefore a jet lying outside the assumed polecap distribution.

#### 4.1.3. Equatorial ring: $\beta_1 = \beta_2 = 90^\circ$

As a contrast, we now consider a model in which all jets lie in the plane of the host galaxy. We plot the quartiles for this model, as well as the  $60\mu\text{m}$  data, in Figure 6. At high values of inclination  $i$ , the quartiles now tend in the direction of decreasing  $\delta$ . This has to be the case, because if the jets all lie in the host galaxy planes, then as  $i \rightarrow 90^\circ$ , we must have that  $\delta \rightarrow 0^\circ$ . From inspection of Figure 6, it is apparent that the data are not uniformly distributed across the quartiles. A KS test indicates that the data are consistent with the model at only the 0.8% level. Thus a model in which all the jets are assumed to lie in the planes of the host galaxies is not compatible with the data.

#### 4.1.4. More general models

We now discuss the more general set of model  $\beta$ -distributions considered above (Section 3.2.1). In these models the jet directions are uniformly distributed over the band on the sky,  $\beta_1 \leq \beta \leq \beta_2$ , where, of course,  $\beta_1 \leq \beta_2$ . Each individual model, in this general set of models, is represented by a point in the  $(\beta_2, \beta_1)$ -plane, and associated with each model (and hence with each point) is a percentage value from the KS test indicating the level of consistency with the assumed model. In Figure 7a and Figure 7b we plot the KS contours in the  $(\beta_2, \beta_1)$ -plane for the whole dataset, and for the  $60\mu\text{m}$  sample, respectively. Note that the permitted areas of the diagrams are bounded by the line  $\beta_2 = \beta_1$  and by the line  $\beta_2 = (\text{sup } \beta_{\min})$ , where  $\text{sup}(\beta_{\min})$  is the largest value of  $\beta_{\min}$  in the sample and is equal to  $75^\circ$  for the whole dataset, and to  $65^\circ$  for the  $60\mu\text{m}$  sample.

We find that a broad range of models is permitted by the datasets, and note that as commented earlier, although use of the serendipitous data, in addition to the  $60\mu\text{m}$  sample, doubles the number of data points, it does not result in correspondingly (or even, significantly) greater constraints on the permitted models. It is evident that permitted models are insensitive to the value of  $\beta_2$  (within the permitted set of values) but favor values of  $\beta_1$  which are less than around  $50^\circ - 60^\circ$ . Thus large zones of avoidance are not favored by the data, but otherwise, as long as  $\beta_2$  is big enough (that is, as long as jets are not excluded from lying in regions too close to the host galaxy planes) all models are reasonably consistent with the data.

## 4.2. Using near side/far side information

Up until now, we have made no assumptions about the orientation of the jet, other than it is a quasi-linear structure that can be described by a position angle. (It has not, for example, been necessary to know at which end of the jet the nucleus lies). In most cases, however, it is possible to locate the nucleus and to see that the jet is either one-sided or highly asymmetric in brightness. It is unlikely that this asymmetry results from relativistic boosting (e.g. Ulvestad et al 1999) and so one is left with the possibility that the jets are intrinsically asymmetric (or even one-sided), or that the radio emission can be seen only if the jet interacts with interstellar gas, or else, that the counter-jet is somehow partially concealed by intervening material. The latter possibility appears to be the case for jets on parsec scales (Ulvestad et al 1999), where the density of ionized material required for significant free-free attenuation is consistent with measured X-ray absorption columns. In the few cases where larger scale jets have been simultaneously imaged in the radio continuum and in HI 21 cm absorption, it is found that absorption peaks on the side of the fainter (or less coherent) jet (Gallimore et al 1999 and references therein). In these cases at least, it would appear that obscuration (possibly by free-free absorption) may play a role in rendering the counter-jet less visible. Given that there are no working models for the generation of intrinsically one-sided jets, we now adopt as a tentative working hypothesis the notion that the brighter jet is the one that lies above the host galaxy plane (as seen from the Earth). If, *and only if*, we make this hypothesis, we can utilize the information (which we have for some galaxies) as to whether the dominant jet is projected against the near/farside of the galaxy. The combination of this hypothesis and the near/farside information provides a much finer discriminant between jet models than has been possible thus far. It allows us, for example, to shed some light on the topical issue of Unified Models for Seyfert 1s and Seyfert 2s. We here lay out the method and results of such an analysis and urge future campaigns of HI absorption mapping in Seyfert nuclei in order to subject the hypothesis to direct observational scrutiny. We stress that none of the results discussed thus far (i.e. in Section 4.1) rely upon this hypothesis.

Using the additional information as to whether the observed jet is seen in projection against the near or the far side of the host galaxy plane, and making the additional assumption that the observed jet is the one that lies above the host galaxy plane (as seen from Earth), imposes further constraints on the  $\delta$ -distributions of the galaxies involved (Section 3.2.3). We now use the data of the  $60\mu\text{m}$  sample, including this additional assumption, and compare it (using the KS test) with the models described in Section 4.1.4. The resulting KS contours in the  $(\beta_2, \beta_1)$ -plane are shown in Figure 8. In comparison with Figure 7b, the permitted area is now more restricted by the addition of the extra information and we now require  $\beta_2 \geq 75^\circ$ . In comparison with Figure 7a and Figure 7b, although the level of acceptability of the models is reduced somewhat, it is evident that at the 5%-level (corresponding to  $2\text{-}\sigma$  on a normal distribution) the favored region has not changed to any great extent, especially as far as  $\beta_1$  is concerned.

#### 4.2.1. Distinguishing Seyfert 1s and Seyfert 2s

Since, by adding the additional information about whether the jet is seen in projection against the near or far side of the galaxy, the formal acceptability of the models has been reduced (although the models are still acceptable), we now investigate which feature of the data is causing the additional problem. In particular, we wish to test the assumption we have used so far, which is that the property of being a Seyfert 1 or a Seyfert 2 is intrinsic to the galaxy, and does not depend on viewing angle. If this hypothesis is correct, then we should be able to obtain estimates of the  $\beta$ -distributions for the Seyfert 1s and Seyfert 2s separately. In Figure 9a we plot the KS acceptability contours using the data from the  $60\mu\text{m}$  sample for the Seyfert 2s alone. Apart from the constraints that  $\beta_2 \geq \beta_1$  and that  $\beta_2 > \beta_{\text{min}}$  almost all of the permitted region of parameter space is acceptable, although, as found for the Seyfert 1s and 2s combined (Figure 8), smaller values of  $\beta_1$  (that is smaller excluded polecaps) are preferred.

When we plot the contours for the Seyfert 1  $60\mu\text{m}$  data alone, however, (Figure 9b) it is clear that there is a problem. Here the maximum acceptability level is only 7%. Most of the permitted region of parameter space has acceptability levels less than 5% (equivalent to  $2\text{-}\sigma$  on a normal distribution), and the model in which the jets are oriented randomly with respect to the host galaxy is acceptable only at the 3% level. In technical terms, the low level of acceptability has come about because all of the eight Seyfert 1s in this sample have  $\delta > 35^\circ$ , and because three of them have the jet seen in projection against the near side of the galaxy. If a jet is seen in projection against the near side of a galaxy, then for that galaxy low values of  $\delta$  are much more probable than high values. This is because, for near side jets, the arc lengths,  $|\phi_1|$ , of the great circles along which the jet axis is restricted to lie (by the combination of  $i$  and  $\delta$ ) are shorter if  $\delta$  is larger. Thus the models predict low values of  $\delta$ , and the data contain a preponderance of high values of  $\delta$ .

### 4.3. Viewing restrictions for Seyfert 1s and 2s

Thus, we have found that our assumption that a Seyfert 1 is seen as a Seyfert 1, no matter from which direction it is viewed, has led us into an inconsistency (albeit a fairly mild one). In the light of current wisdom, the fact that a Seyfert 1 might not be seen as Seyfert 1 from all viewing angles does not come as a surprise, but this is, to our knowledge, the first time that such an inconsistency has been demonstrated directly in a general way, from the data on a large statistical sample of galaxies. In addition it is evident from our data where the problem lies, and that is with the long great circle arcs (and corresponding high probabilities) associated with low values of  $\delta$ . There is a straightforward way of rectifying this problem, and this is to truncate the arcs in some way. Taking current wisdom into account, we can do this by adding the hypothesis that an AGN only appears as a Seyfert 1 if the angle  $\phi$  between the jet axis and the line of sight is less than some value  $\phi_c$ . We do not have enough data to determine the value of  $\phi_c$  with any accuracy, and

so we adopt a value of  $\phi_c = 40^\circ$  as being consistent with the ratio of Seyfert 1s to Seyfert 2s in our own data, as well as being consistent with previous estimates (e.g. Osterbrock & Shaw 1988; Osterbrock & Martel 1993). This is also consistent with the fact that, in the  $60\mu\text{m}$  sample, there is a much larger proportion of unresolved radio sources in Seyfert 1's compared to Seyfert 2's, and that their average radio extent is smaller.

If we make this additional assumption, then the acceptability contours, using the KS test, for the Seyfert 1s alone is shown in Figure 10. The region of permitted values is now bounded as before by requiring  $\beta_2 > \beta_{\min}$ , but now also by requiring  $\beta_1 < \beta_{\max}$ . The value of  $\beta_{\max}$  comes about because the additional restriction  $|\phi| < \phi_c$ , means that for each galaxy, with given  $(\delta, i)$ , there is a largest value that  $\beta$  can take. In order for all the galaxies in the sample to be able to have jet axes such that  $\beta_1 \leq \beta \leq \beta_2$ , we therefore require that  $\beta_1$  be less than some quantity  $\beta_{\max}$ . We see from Figure 10, that most of the permitted region of parameter space is now acceptable. For example, the model with randomly oriented jets is acceptable at the 18% level.

However, if we make the stronger assumption that all AGN with  $|\phi| < \phi_c$  are Seyfert 1s, we have an immediate conflict with the data. This comes about because of the properties of one object, NGC4388. This object has  $i = 70^\circ$ ,  $\delta = 70^\circ$ , and therefore  $|\phi_1| = 21^\circ$ . In addition, the jet in this system is projected against the near side of the galaxy. Therefore, we must have (given our assumptions)  $|\phi| \leq 21^\circ$ . Thus, by our assumptions so far, this object should be a Seyfert 1. In fact, it is a Seyfert 2. We are therefore drawn to the conclusion that the simple hypothesis that all AGN with  $|\phi| < \phi_c$ , for some value of  $\phi_c$  are Seyfert 1s, and the rest are Seyfert 2s, cannot be sustained.

We note, however, that the problem came about for a galaxy which had a large value of inclination  $i$ . Indeed, returning to Figure 3b, we can see that all the galaxies with large values of  $i$  are Seyfert 2s. Again, drawing on current wisdom (Keel 1980; Lawrence & Elvis 1982; Maiolino & Rieke 1995; see the discussion in Antonucci 1999), this leads us to introduce the additional hypothesis that an active nucleus seen in a galaxy with high inclination,  $i > i_c$ , for some value  $i_c$ , is always identified as a Seyfert 2, independent of the jet orientation relative to the line of sight. We cannot measure the value of  $i_c$  from the data, but the data do require that  $i_c \gtrsim 60^\circ$ .

An observation that corroborates this proposition is the detection of several highly inclined Seyfert 2 galaxies in our sample, without extended radio emission (MRK607, IRAS04385-0828, UGC12348, IRAS13059-2407, and NGC3281). From the point of view of the Unified Model, we would expect to see Seyfert 1's with unresolved, or smaller extended radio emission than Seyfert 2's, because they are seen pole-on. As discussed in Section 2.1, 50% of the galaxies in the  $60\mu\text{m}$  sample do not show extended radio emission, and  $\approx 2/3$  of these galaxies are Seyfert 1's, which is consistent with the predictions. In this way, the observation of highly inclined, unresolved Seyfert 2's is consistent with the proposition that galaxies will always be classified as Seyfert 2's if they have high inclination, irrespective of the angle between the jet and the line of sight.

Combining all these ideas, we construct the following model. We assume that an AGN is seen

as a Seyfert 1 only (i) if it is seen with jet axis close enough to the line of sight ( $|\phi| < \phi_c$ ; we adopt  $\phi_c = 40^\circ$ ), and (ii) if it is seen from sufficiently far out of the plane of the host galaxy ( $i < i_c$ ; we adopt  $i_c = 60^\circ$ ). Otherwise, the AGN is seen as a Seyfert 2. Adopting this hypothesis, we can now construct models for the  $\beta$ -distributions and compare them with the data. In Figure 11, we plot the consistency levels for the  $60\mu\text{m}$  sample. (Note that this combined hypothesis enables us to combine all the data, using both Seyfert 1s and Seyfert 2s.) We find that all of the permitted region is acceptable, and the preference still is for low values of  $\beta_1$  and high values of  $\beta_2$ . The model with randomly oriented jets is acceptable at the 76% level. We note here that a similar model was favored by the analyzes of Nagar & Wilson (1998).

#### 4.4. Selection Effects

Until now, as we mentioned earlier, we have made the assumption that the objects in our sample are representative of the set of Seyfert galaxies as a whole. Because of selection effects, however, this may not be the case. Here we consider briefly what these selection effects might be, and to what extent they might effect the conclusions of our paper. We consider in turn the possibilities of, and implications for, selection effects in  $i$ ,  $\delta$ ,  $\beta$ , and  $\phi$ .

##### 4.4.1. Selection effects in $i$

As we noted above, (see Figure 3a and Figure 3b) the sample is apparently deficient in objects at large values of the inclination,  $i$ . For example, for randomly oriented galaxies one expects half of the sample to lie at  $i > 60^\circ$ , whereas for the  $60\mu\text{m}$  sample only 13/33 lie in that range. However, as we emphasized above, the method we have adopted for estimating the distribution of jets in  $\beta$  does not rely on completeness of the sample in  $i$ . The method is still valid even if all the galaxies in the sample had the same value of  $i$ . However, as we have seen, galaxies with larger inclinations provide much better discriminants between the various possible model distributions in  $\beta$ . Thus a sample, such as the  $60\mu\text{m}$  sample, which contains a relatively high fraction of galaxies at high inclination, is particularly valuable for our current purposes.

##### 4.4.2. Selection effects in $\delta$

The radio position angle and the position angle of the host galaxy's major axis are determined by different methods and at different wavelengths. Thus it is difficult to envisage any selection effect which might preferentially populate, or exclude, any particular range in  $\delta$ . Thus any selection effects here are really physical.

#### 4.4.3. Selection effects in $\beta$

What we address here is whether a particular value of  $\beta$  for a host galaxy might render that galaxy to be more, or less, likely to be included in our sample. For example, what we require for inclusion is that we are able to detect a radio jet. Thus we require the radio source to be bright enough and to display sufficient extension. It is possible that these qualities do depend on the direction in which the jet emerges from the nucleus. For example, if the jet emerges close to the galaxy plane (large  $\beta$ ) it might be that it impinges upon more material and so appears brighter, thus increasing the probability of inclusion in the sample. Conversely, such a jet, because it meets more material might be unable to propagate so far, and thus fail to be detected as an elongated source, and so fail to qualify for inclusion in the sample. Since it is not evident whether this effect works for, or against, inclusion, it is not obvious what remedial action might be taken.

#### 4.4.4. Selection effects in $\phi$

The angle  $|\phi|$  is the angle between the jet axis and the line of sight. Given current ideas about the AGN environment, towards which we have been drawn by the present dataset, it is evident that objects with low values of  $|\phi|$  (and low values of inclination  $i$ ) are ones in which the nucleus is directly observable, and are therefore more likely to be detected. In contrast, for a given set of intrinsic jet sizes, it is those jets which are nearly at right angles to the line of sight ( $\phi \simeq 90^\circ$ ) which would be preferentially included in the sample. Thus we can identify two selection effects which operate in different directions as far as values of  $\phi$  are concerned.

The  $60\mu\text{m}$  sample is chosen using a brightness limit at  $60\mu\text{m}$ , and an additional color criterion using the ratio of  $25\mu\text{m}$  to  $60\mu\text{m}$  fluxes; de Grijp et al (1987). Because the hypothetical molecular torus is believed to emit more isotropically at longer wavelengths (Pier & Krolik 1992; Efstathiou & Rowan-Robinson 1995), it is hoped that such selection criteria would help to minimize the effect of inclusion in the sample depending on the viewing angle of the object. A secondary consequence of this selection criterion has been that by using far infrared discriminants we have been able to include in the sample a relatively large number of galaxies at high inclination.

Thus the main selection effect of which we are aware is the problem of resolution of the nuclear radio source into an elongated structure (jet), and the fact that an intrinsically elongated source is more easily resolved if  $\phi \simeq 90^\circ$ . In order to examine this effect more closely we separated the  $60\mu\text{m}$  sample (which of course only includes those objects which are resolved at radio wavelengths) into two equal sample of 17 objects, sorted according to distance (redshift). In Schmitt et al (2000) we have shown that there is no strong dependence of intrinsic length of jet on  $60\mu\text{m}$  luminosity. Under these circumstances, we might expect the further set of objects to be closer to the resolution limit (that is to have values of  $\phi$  closer to  $90^\circ$ ) than the nearer set. If true, then we might expect that the  $(i, \delta)$ -distributions of the two sets might differ in some systematic way. As far as we can tell this is not the case.

Alternatively, if it happened that this selection effect (the hypothetical increased radio resolvability for high  $\phi$ ) was so dominant that it overrode all other considerations (so that for each galaxy included in the sample we know that  $\phi = 90^\circ$ ), then we would be able to determine  $\beta$  for each galaxy, and thus determine the  $\beta$ -distribution directly. We plot the resultant distribution in Figure 12. We see from the Figure that the distribution is consistent with being uniform in  $\cos \beta$ , which corresponds to jet orientations being independent of the host galaxy. We stress that this is not a sensible method for deriving the  $\beta$ -distribution of Seyfert jets, since  $\phi = 90^\circ$  is not a good assumption for nearby galaxies, nor for those galaxies with intrinsically long, and so easily resolved, jets. Nevertheless, this exercise does demonstrate that the extreme assumption that all jets lie in the plane of the sky ( $\phi = 90^\circ$ ), does not lead to results that are radically different from those we have obtained above.

#### 4.5. Summary of findings

In this Section, for convenience, we summarize our results.

We have analyzed the data under the assumption that the galaxies in our sample have been randomly selected from a set of galaxies whose jet directions are distributed uniformly in azimuth about the normal to the galaxy disk plane. We have then also assumed that the underlying set of galaxies from which our sample has been selected has a particular distribution in  $\beta$ , the angle between the jet and the galaxy normal. We find that an adequately general set of model distributions is given by assuming that galaxy jets are uniformly distributed over the galactic sphere in an azimuthal band  $\beta_1 < \beta < \beta_2$ . We then apply a KS test to give (loosely speaking) the probability that the hypothesis that our sample is drawn from the assumed model distribution is valid.

##### 4.5.1. Analysis with no extra assumptions

First we consider the whole dataset, displayed in Figure 3a and Figure 3b, and make no use of additional information such as whether an AGN is a Seyfert 1 or 2, or whether we have information about the jet being projected against the near or far side of the galactic plane. Thus we are making the assumption here that, in contradiction to the unified model, classification of an object as a Seyfert 1 or Seyfert 2 is independent of the angle  $\phi$  between the jet and the line of sight.

Under these assumptions we find, using the data from the  $60\mu\text{m}$  sample, and taking the data for both Seyfert 1s and 2s together (Figure 7b), that the data are compatible with the jets being randomly oriented relative to the host galaxy ( $\beta_1 = 0^\circ$ ,  $\beta_2 = 90^\circ$ ) at the 67% level. The data are also consistent with the jets being distributed in uniform polecaps as long as the cap is large enough to encompass the galaxy with the largest value of  $\beta_{\text{min}}$ . Thus models with

$\beta_1 = 0$ ,  $\beta_2 > \beta_{\min}$  are equally acceptable. In addition models with excluded regions around the pole ( $\beta_1 > 0$ ) are also acceptable, as long as the region of exclusion, i.e.  $\beta_1$ , is not too large. For example the probability that the data is drawn from a model with  $\beta_1 = 60^\circ$ ,  $\beta_2 = 90^\circ$  is less than 5%. These conclusions are essentially unchanged (Figure 7a) if we use the whole dataset, adding the serendipitous sources to the  $60\mu\text{m}$  sample.

#### 4.5.2. Using near side/far side information

In addition to the assumptions of Section 4.5.1, we now add the premise that the observed jet (or the dominant jet, in the case of a two-sided jet) is the one which lies above the disk plane of the host galaxy (as seen from Earth). We then make use of the observational data which enables us to ascertain (for a number of galaxies) whether the jet is seen in projection against the near side or the far side of the galaxy plane. We then use this knowledge as a further constraint on the jet direction.

Using, again, just the  $60\mu$  sample, we find:

(i) If we use all the data (combining Seyfert 1s and 2s) then only models with  $\beta_1 \gtrsim 45^\circ$  are inconsistent with the data at the 5% level, as long as we choose  $\beta_2 > \beta_{\min} = 75^\circ$  (Figure 8). Thus, for example, the data are consistent with randomly oriented jets. The conclusions are similar, if we use just the data for the Seyfert 2s alone (Figure 9a).

(ii) However, if we consider the Seyfert 1s alone, then there is a problem finding compatibility with the simple models we have used so far (Figure 9b). The problem arises because all 8 of the Seyfert 1 galaxies have  $\delta > 35^\circ$ , and because of these 8, at least 3 have the jet projected against the nearside of the galaxy. For these 3 galaxies, the jet axis must (according to our assumption) lie on the short arc of the great circle between the line of sight and the galactic plane. For such galaxies, the predicted distribution of  $\delta$  for any  $\beta$ -distribution, is heavily weighted towards small values of  $\delta$ , because the arc length,  $|\phi_1|$  is largest for small values of  $\delta$ . This contrasts with the finding that  $\delta > 35^\circ$  for the data set as a whole, and  $\delta > 43^\circ$  for the 3 nearside galaxies. We find that the optimal model is for jets oriented in a narrow band along the galactic equators, and that even this model is inconsistent with the data at the 7% level. Most of the permitted parameter space is excluded at the 5% ( $2\text{-}\sigma$ ) level.

#### 4.5.3. Need for further restrictions - a generalized unified model

The problem with the Seyfert 1 galaxies, discussed in Section 4.5.2, comes about because, for galaxies whose jets are projected against the near side of the galaxy plane, great circles with low values of  $\delta$  have the longest arcs. The inconsistency can, therefore, be circumvented if the arc lengths can be truncated. One way of doing this is to invoke the unified model for Seyfert 1s and

2s, which makes the additional assumption that any Seyfert viewed with angle,  $\phi$ , between jet axis and line of sight small enough, i.e.  $|\phi| < \phi_c$ , is a Seyfert 1. As an example, which is consistent with other aspects of our and other datasets, we take  $\phi_c = 40^\circ$ . Then adding the restriction that all Seyfert 1s have  $|\phi| < 40^\circ$  we find that a wide range of models, including the randomly oriented model, are consistent with the data (Figure 10).

However, the converse of this assumption, that all Seyfert 2s have  $|\phi| > 40^\circ$  is then not consistent with the data. The problem arises because of NGC4388, which has the jet projected against the near side of the galaxy plane, and for which  $|\phi_1| = 21^\circ$ . This implies that for this galaxy  $|\phi| < 21^\circ$ , and therefore, according to our hypothesis, this galaxy should be a Seyfert 1, however, it is a Seyfert 2. Thus the application of the simple unified model, just in terms of  $\phi_c$  leads to a contradiction with the data.

If we are prepared to make one more assumption, then there is a way out of this dilemma. We note from Figure 3b that all Seyfert 1 galaxies have  $i < 60^\circ$ . In addition, the galaxy NGC4388, which gives rise to the contradiction has  $i = 70^\circ$ . We therefore arrive at the following hypothesis:

If a galaxy has  $|\phi| < \phi_c$  (where we adopt  $\phi_c = 40^\circ$ ), and has  $i < i_c$  (where from the data we conclude  $i_c \geq 60^\circ$ , and we adopt  $i_c = 60^\circ$ ), then it is seen as a Seyfert 1; if either of these conditions is not met, then the galaxy is seen as a Seyfert 2.

Under this hypothesis, the data is consistent with a large range of models, and, in particular, the most general models of random jet orientations is fully acceptable (Figure 11).

## 5. Implications for feeding the nucleus

Most of the gas in a spiral galaxy is in the plane of the galaxy. Any gas added to a spiral galaxy is likely to rapidly end up in the galaxy disk – either by direct collision with gas already there, or by settling in the galaxy potential to the extent that it is axisymmetric and disk-like, rather than spherical. Thus the simplest expectation for gas flow into the nucleus of a spiral galaxy would be that gas arriving at the central black hole would do so with angular momentum vector perpendicular to the disk of the galaxy. Since jets are expected to be launched perpendicular to the central disc, the simple hypothesis and expectation is that all jets in spirals should be perpendicular to the disk plane. This expectation is flatly contradicted by observations. Indeed we have shown above that a completely random orientation of the jets with respect to their host galaxies is consistent with all the data. In the light of this, we now discuss the implications of our findings for the means by which the central black hole is fed in Seyfert nuclei, and in other active galactic nuclei.

There seem to be two general approaches to explaining the mismatch between the angular momentum vectors of the galaxy disk and the central accretion disk.

### 5.1. Aligned gas inflow from the galaxy disk

First, one can assume that the matter is indeed fed to the nucleus from the visible gas reservoir in the galaxy disk. The mechanisms by which this might be accomplished have been discussed by a number of authors, and possibilities include tidal interactions (Byrd et al., 1986; Hernquist & Mihos, 1996) and bar driven inflow (Shlosman et al., 1989; Thronson et al., 1989; Mulchaey & Regan, 1997). Recent work on the environments of Seyfert galaxies seem to imply that minor mergers (that is, the merging with the Seyfert host galaxy of a much less massive, but gas-rich, companion) might play a prominent rôle in triggering Seyfert activity (De Robertis et al, 1998a,b; Dultzin-Hacyan et al 1999). We should note, however, that doubts have been raised as to whether such mechanisms can actually deliver gas to the nucleus of the galaxy and so excite activity, because the presence of an inner Lindblad resonance can act to choke off inward gas flow (Sellwood and Moore, 1999). But, however the delivery of gas to the nucleus is achieved, it is evident that in this case the gas reaching the nucleus should have angular momentum vector parallel to that of the bulk of the gaseous disk of the galaxy. In this case, therefore, some means must be found to warp the disk between where matter is added at the outside and where the jet is produced at the inside. The obvious possibilities here are:

#### 5.1.1. *Warping due to self-irradiation instability*

Pringle (1996, 1997) has shown that an accretion disk around a compact object such as a black hole is unstable to warping, caused by photon back-pressure from the unevenness of the disk’s self-illumination. For an AGN disk he estimates that the warping might occur at radii as small as 0.02 pc and on a timescale of around  $10^6$  years. He found that the disk plane in the inner regions of such a disk might in general bear little relation to the outer disk plane, and also that the disk shapes could be such that photons from the center might only emerge in a pair of narrow cones and that the cones might in general not be necessarily simply aligned with either the inner or the outer disk. Thus the naive conclusions from these simple calculations are that a) there is likely to be little relationship between the plane of the outer disk and the direction of the jets, and b) ionization cones which emerge from these disks need not be centered on the jet directions. However, Pringle also stressed that these simple calculations underestimate the strength of the effect by only taking photon momentum (rather than wind momentum) into account, and that they also neglect various other effects such as: the effect of self-irradiation on the structure of the disk, self-gravity in the disk, the effect of the central jet striking the disk when the warp exceeds 90 degrees, and the major uncertainties about the time-dependent behavior of a warped accretion disk, including uncertainties about the viscous processes themselves (Ogilvie 1999).

### 5.1.2. *Warping by the Bardeen-Petterson effect*

The dragging of inertial frames by a rapidly rotating black hole leads to the inner regions of the disk being forced to precess differentially about a vector parallel to the spin axis of the black hole. Then viscous dissipation of the disk twist so caused leads to the inner disk regions being aligned with the spin of the black hole (Bardeen & Petterson, 1975). Then the jet/galaxy disk misalignment could be explained if the black hole spin is misaligned with that of the galaxy disk. For this to be a plausible explanation we need to be able to answer the two questions: Why should the black hole be rapidly rotating and why should its spin be misaligned? If the self-irradiation instability discussed above is operative, it is no longer clear that accretion from a disk will necessarily lead to spin-up of the hole, because the incoming disc at the center wanders in orientation. Thus the simplest way for the central black hole to be spun-up *and* misaligned is for it to accrete a black hole from the nucleus of a captured galaxy (Wilson and Colbert, 1995, and see below). Note that the accreted black hole need only be, say, 0.1 - 0.2 of the original host mass for spin-up and misalignment to take place because, in the final stages of the black hole merger, the orbital angular momentum of the merging black holes gets subsumed into the spin of the remnant. However, the long term effect of feeding a misaligned black hole from the steadily oriented disk is to align the black hole with the disk, and the timescale for doing so is faster than the mass growth timescale of the hole by about two orders of magnitude, and may be even faster. This is because angular momentum transfer between the hole and the disk takes place at a large radius in the disk (Scheuer & Feiler 1996), and because warp is propagated through an accretion disk much faster than mass or (aligned) angular momentum (Papaloizou & Pringle, 1983; Kumar & Pringle, 1985; Natarajan & Pringle 1998).

### 5.1.3. *Warping by a misaligned gravitational potential*

The central black hole appears to be surrounded by a nuclear star cluster both in early-type galaxies (Gebhardt et al., 1996; Faber et al., 1997; van der Marel, 1999) and in spiral galaxies (Carollo & Stiavelli, 1998; Carollo, 1999), where the mass of the cluster begins to dominate the mass of the hole at a radius of a few tens of parsecs. If the star cluster is axi-symmetric (rather than spherically symmetric, see the discussion by Merritt & Quinlan, 1998) and has its symmetry axis misaligned with the galaxy disk, and if the degree of non-sphericity is sufficiently great, then it would be possible for tidal potential of the cluster to induce differential precession in the disk. This, coupled with viscous dissipation of the disk twist so induced, would act to align the disk with the symmetry axis of the cluster.

The cause of such a misalignment might be some form of minor merger, discussed in more detail below (Section 5.2.1). There are two reasons, however, why a misaligned central star cluster may not be the answer. First, the work by Carollo (Carollo et al, 1997; Carollo & Stiavelli, 1998, Carollo, 1999) on the structure of the centers of spiral galaxies indicates that there is a tendency

for late-type spirals to contain exponential disk-related bulges around the central star cluster. This supports scenarios in which bulge formation occurs relatively late, in dissipative accretion events driven by the disk. If so, it seems likely that the central star cluster, formed as part of the same process, would be aligned with the disk. Second, if it does appear that the stellar kinematics of the nuclear region does provide the explanation of the jet/galaxy misalignment found in Seyferts, it would be in stark contrast to the finding (Van Dokkum & Franx, 1995; Section 5.2) that in early-type galaxies the jet direction is determined by the angular momentum of the incoming material, and not by the stellar rotation axis.

## 5.2. Misaligned gas inflow

Second, one can assume that the disk is not fed from the obvious gas reservoir of the disk of the spiral galaxy, in which case the problem of alignment does not (necessarily) arise. In this context it is worth noting the survey of dust in the cores of early type galaxies by Van Dokkum & Franx (1995). They find that dust disks are present in a high fraction of these galaxies, indicating (perhaps) that minor mergers occur quite frequently, and also find that the detection rate is higher in radio galaxies, indicating (perhaps) a connection between the presence of dust and nuclear activity. The overall finding is that the dust plane is not in general relaxed to any symmetry plane of the galaxy, but that the dust plane is in general perpendicular to the radio axis, if there is one. This finding is consistent with the results of surveys of 3CR radio-galaxies by de Koff et al. (1999), and by Martel et al. (1999). The simplest interpretation of this is that the dust plane is the debris trail of a small merger incident, and that the direction of the radio jet is determined by the orbital plane of the incoming mergee. This result has implications for the foregoing discussion. First, the jet axis in these early-type radio galaxies seems to be determined by outside influences, and not by the intrinsic spin of the black hole (unless, either each minor mergee brings in a small nuclear black hole of its own and tweaks the central black hole into line, or the disk accretion is very efficient at aligning the black hole with the disk itself, Natarajan & Pringle, 1998). Second, the self-irradiation instability (Pringle 1996,1997) appears not to be operative in these systems. And, third, jet direction does not appear to be determined by asymmetries in the potential of the host galaxy.

We now consider various processes which might give rise to misaligned gas flow to the central regions.

### 5.2.1. *Misaligned minor mergers*

Misaligned gas in the center of a spiral galaxy, could be provided as the result of small scale cannibalism, whereby a small, gas-rich galaxy is accreted on a trajectory which goes more or less straight to the nucleus (if the trajectory of the small mergee intersects the symmetry plane of

the spiral, it seems likely that the gas in the mergee would be stripped by interaction with the spiral’s gaseous disk). The misaligned accreting gas needs to be provided by the small galaxy participating in this minor merger event. This cannot be a large scale merger of two comparable mass systems, such as for example Arp 220 where counter-rotating gas disks are seen around the two original nuclei which have yet to merge (Sakamoto et al., 1999), because the resulting galaxy is then elliptical rather than spiral (Barnes and Hernquist, 1992,1996), and because Seyferts are simply not in rich enough environments (De Robertis et al 1998b).

There is increasing evidence that the kinematics in the nuclei of spiral galaxies is not simple – for example, the evidence for counter-rotation in the core of the Galaxy (Genzel et al 1996), the multiple nuclei in M31 (Stark & Binney, 1994; Tremaine, 1995; Sil’chenko, Burenkov, & Vlasyuk, 1998), and the results of a HST high resolution imaging surveys of nearby Seyferts (Malkan et al., 1996), and of nearby spiral galaxies (Carollo, 1999). In addition there is an increasing number of instances of complex gaseous and stellar kinematics in the nuclei of S0 and spiral galaxies, including misaligned and counter-rotating discs of gas and stars (Rubin, 1994; Galletta, 1996; Kuijken, Fisher and Merrifield, 1996; Sil’chenko et al., 1997; Zasov & Sil’chenko, 1997; Garcia-Burillo et al.,1998; and Sil’chenko, 1999). However, even though (Carollo, 1999) the brightest nuclei embedded in spiral galaxies with an active (AGN or HII-type) ground-based central spectrum are surrounded typically at HST resolution by complex circum-nuclear structure (e.g. spiral arms, star-forming rings, spiral-like dust lanes), there is little evidence that this structure is severely misaligned with the main galaxy disk.

From a theoretical point of view, an interesting calculation which needs to be carried out in this context is to calculate where the large/small merger border lies. The main problem here is to calculate how accurate the initial trajectory needs to be for the gas associated with the incoming small galaxy to reach the nucleus of the Seyfert host with its orbital angular momentum intact. Calculations of small scale cannibalism have yet to be carried out for incoming gas-rich galaxies on arbitrary orbits. Calculations have been carried out for incoming galaxies on coplanar orbits in both the aligned and counter-aligned cases (Thakar & Ryden, 1998), who find, for example that the accretion of massive counter-rotating disks drives spiral galaxies towards earlier (S0/Sa) Hubble types. In addition, N-body calculations of minor mergers with disk galaxies (neglecting the hydrodynamics) have been carried out by Velázquez and White (1999). One simple expectation would be that for each direct hit, there are many more misses whose orbits intersect the disk of the galaxy. This would be likely to merge the gas in the small mergee with the gas already in the spiral disk. This might result in feeding the nucleus but the gas reaching the nucleus would in this case be essentially aligned with the spiral disk. We also note that there may be a relationship between the formation of a nuclear ring and the capture of a small counter-rotating satellite galaxy (Thakar et al., 1997). In addition, one expects capture cross-sections for small scale capture to be strongly dependent on the initial orbit (prograde aligned capture is strongly preferred) and one also expects the ability of the mergee to penetrate to depend strongly on its initial central concentration/structure (Velázquez & White, 1999). Moreover it seems that the

distribution of satellite galaxies tends to be anisotropic in that their angular momenta tend to align with the central disk (Zaritsky et al., 1997). Also of interest in this case is what happens to the central black hole (nucleus) of the intruder, if it has one. If this can be captured by the host nucleus before its orbit aligns with the spiral then it might be able to lead to a rapidly spinning and misaligned central black hole (see above).

If this is the predominant mechanism by which activity is initiated in Seyfert galaxies, then, unless each Seyfert we detect has just swallowed its last companion, we would expect to find a strong correlation between Seyfert activity and environment, in that active galaxies should have far more small companions, and should show enhanced evidence of disturbance. Current evidence appears to indicate that Seyfert 1s have a similar number of small companions as the control samples, but that Seyfert 2s do display an enhanced number of small companions (De Robertis et al 1998a,b; Dultzin-Hacyan et al 1999). In addition, Malkan et al (1996) find that the rates for occurrences of bars in Seyfert 1s, Seyfert 2s and non-Seyferts is the same (see also Mulchaey & Regan 1997; Ho, Filippenko & Sargent 1997), but that Seyfert 2s are significantly more likely to show nuclear dust absorption than Seyfert 1s, and tend to reside in galaxies of later type. This is consistent with the tendency for Seyfert 2s at HST resolution to show a disturbed, clumpy morphology (Capetti et al, 1996; Colina et al, 1997; Simpson, et al, 1997).

If the minor merger hypothesis is to be made to work, it may therefore be necessary to argue (c.f. Chatzichristou 1999; Taniguchi 1999) that at an early stage in the merger, the nucleus is more likely to be observed as a Seyfert 2 (with disturbed central regions, large regions of out-of-plane gas, and hence larger extents of NLRs (Schmitt & Kinney, 1996). Later on, the disturbed gas settles more into the galaxy plane, and the nucleus is more likely to be observed as a Seyfert 1. If so, because in a volume limited sample there are about equal numbers of Seyfert 1s and Seyfert 2s, this would mean that the time taken for dynamic evolution of the gas must be about equal to the length of time the Seyfert is active (typically estimated at about  $10^8$  years). In addition, if there is (on average) a time-sequence of Seyfert 1  $\rightarrow$  Seyfert 2, and if the jet/galaxy misalignment is caused by the misalignment of the merger, then one might expect the amount of misalignment to be (on average) less for Seyfert 1s than for Seyfert 2s.

### 5.2.2. *Capture of individual stars or gas from the nuclear stellar cluster*

Capture and consumption of individual stars from the central star cluster by the central black hole has been put forward as a mechanism for feeding the central nucleus (Frank & Rees, 1976; Shlosman et al., 1990). Shlosman et al. (1990) make the case that standard thin accretion disks are not a viable means of delivering fuel to AGN on scales much larger than a parsec because of the long inflow timescales. If activity proceeds on a star by star basis then the orientations of the central disks might be expected to be fairly random. However, if an accretion rate of about a star per year is required, and if the central disk contains tens or hundreds (or more) solar masses then the effects of individual star orbits are going to be averaged out. Even so, if the central

stellar cluster has an anisotropic velocity distribution in the form of a net rotation, then on average we might expect the nuclear accretion disk to be aligned with the central nuclear cluster. As mentioned above, it might well be that the direction of spin of the central stellar cluster is misaligned with the galaxy as a whole.

An alternative possibility is if the source of accreted material is mass loss from the stars making up the nuclear cluster. If matter is lost from the stars in such a way that it can cool and be accreted by the central black hole, and if the nuclear cluster has a net rotation about some axis misaligned with the spin of the galaxy disk, then once again the rotation axis of the central accretion disk need not be correlated with the rotation axis of the galaxy as a whole.

In both these cases, however, there is a question as to whether a sufficient mass accretion rate can be provided to power the observed Seyfert nuclei (Shlosman et al, 1990). Recent calculations of the rates of disruption of stars by massive central black holes (applied to early-type galaxies) indicate that the highest disruption rates are around one star every  $10^4$  years (Magorrian & Tremaine, 1999; Syer & Ulmer, 1999). As a time-averaged rate, this is about two orders of magnitude too low to power standard Seyfert nuclei. However, since the Seyfert phenomenon may well have a duty cycle of only about a per cent, if the stellar disruption rate can be made to be intermittent (for example brought about by dynamical phenomena associated with minor mergers), then this mechanism for feeding the black hole might merit further investigation. Similarly, even if some means can be found for stellar mass loss to be channeled efficiently towards the central black hole, Shlosman et al (1990) argue that time-averaged gas production rate from Population II (aged stars) is  $\sim 10^{-5}M_{\odot}$  per year per  $10^6M_{\odot}$  of stars. Once again this would give an inadequate mass accretion rate to power Seyfert nuclei. However, there is increasing evidence in terms of the nuclei being chemically distinct stellar sub-systems (Sil’chenko, 1999; Sil’chenko et al., 1999) and in terms of recent star formation (Genzel et al., 1996; Ozernoy et al., 1997; Davidge et al 1997a,b) that the possibility of sporadic enhanced mass loss from stars in the nuclear cluster might be worth further investigation as a source of fuel for Seyfert nuclei.

### 5.2.3. *Capture of individual molecular clouds from the host galaxy*

An alternative possibility is if the gas flow onto the nucleus comes from the capture and consumption of individual molecular clouds from the host galaxy. Evidence from the center of our Galaxy in the form of young stars showing a rotation axis misaligned with the galactic plane (Genzel et al., 1996), demonstrates the possibility of gas arriving in the neighborhood of a nucleus with misaligned angular momentum. In this case the amount of star formation produced is about what one might expect from the arrival of a single molecular cloud. If the ensemble of molecular clouds in a galaxy has a positional and velocity distribution such that the scale-height of the cloud layer is larger than the tidal radius of the clouds (typically about 100pc for a black hole mass of  $10^8M_{\odot}$ ) then just as in the case of stars accreting individually from a central star cluster (see above) the angular momenta of accreted clouds could point in fairly random directions. Even

so, it seems unlikely that the molecular cloud distribution is completely unrelated to the galactic plane, and so in this case too one might expect to see some relationship between disk direction and galactic plane.

## 6. Summary

In this paper we presented the study of the relative angle between the accretion disk and the galaxy disk for active galaxies hosted by spirals (Seyferts), using a sample selected by a mostly isotropic property, the flux at  $60\mu\text{m}$ , and warm infrared colors. This sample consists of 88 galaxies (29 Seyfert 1's and 59 Seyfert 2's), 33 of which show extended radio emission and are not in interacting systems (8 Seyfert 1's and 26 Seyfert 2's). Our study used VLA 3.6cm data taken by us, archival VLA data, ground based B and I images of the galaxy disks, as well as long slit spectroscopy. All the data were observed, reduced and analyzed in a similar way, to ensure a homogeneous dataset and minimize, as much as possible, selection effects. For parts of the analysis we also used an enlarged sample, which includes the 33 galaxies from the  $60\mu\text{m}$  sample, plus 36 serendipitous Seyfert galaxies selected from the literature, giving a total of 69 galaxies (20 Seyfert 1's and 50 Seyfert 2's). Most of the data for the serendipitous sample was obtained from the literature and not measured homogeneously as for the  $60\mu\text{m}$  sample.

For each galaxy we had a pair of measurements  $(i, \delta)$ , where  $i$  is the galaxy inclination relative to the line of sight and  $\delta$  is the angle between the jet projected into the plane of the sky and the host galaxy major axis. For some of the objects, we also had the information about which side of the galaxy is closer to Earth, obtained through the inspection of dust lanes or from the rotation curve, assuming that the spiral arms are trailing. This information was used together with a statistical technique developed by us, to determine the distribution of angles  $\beta$ , the angle between the jet and the host galaxy rotation axis. This technique tests different  $\beta$ -distributions in the range  $\beta_1 \leq \beta \leq \beta_2$ , to determine which range of parameters  $\beta_1$  and  $\beta_2$  produces the most acceptable models.

From the assumption that the of a homogeneous  $\sin \beta$  distribution in the range  $0^\circ \leq \beta \leq 90^\circ$  and not differentiating between Seyfert 1's and 2's, we showed that the observed data and the models agree at the 67% level for the  $60\mu\text{m}$  sample and 81% level for the total sample ( $60\mu\text{m}$  plus serendipitous sources). Using only a polecap ( $0^\circ \leq \beta \leq 65^\circ$ ) we showed that the model and  $60\mu\text{m}$  data agree at the 69% level, while for an equatorial ring ( $\beta_1 = \beta_2 = 90^\circ$ ) there is a bad agreement, only at the 0.8% level. Using a more general model, we tested which range of values  $\beta_1$  and  $\beta_2$  (where  $\beta_1 \leq \beta_2$ ) are acceptable. This showed that, independent of the sample ( $60\mu\text{m}$  or total),  $\beta_2$  has to be larger than  $65^\circ$ - $75^\circ$ , and the acceptability of the models does not depend strongly on this value, but for  $\beta_1$  the agreement is better for values smaller than  $40^\circ$ - $50^\circ$ . The addition of the information about which side of the galaxy is closer to Earth, and if the jet is projected against the near or the far side of the galaxy, shows that the acceptable parameter range does not change considerably, but the maximum acceptability of the models was reduced. As discussed in Section

4.2, this result depends on the assumption that the dominant jet lies above the galaxy plane (as seen from Earth). We plan to test this hypothesis observing HI and free-free absorption against the weaker side of the radio jets.

An important result from our analysis appeared when we distinguished between Seyfert 1’s and Seyfert 2’s. The Seyfert 2’s still have a good agreement with the models, and all the permitted  $\beta_1 - \beta_2$  parameter space is accepted at the  $2\sigma$  level or higher. However, when we consider only the Seyfert 1’s, the agreement is poor, with the maximum acceptability being only 7%. In order to solve this problem, we introduced a viewing angle restriction to the models, which is, a galaxy can only be recognized as a Seyfert 1 if the angle between the jet and the line of sight  $|\phi|$  is smaller than a given angle  $\phi_c$ . We chose  $\phi_c = 40^\circ$  based on information from the literature, and show that this assumption increases the acceptability of the models. This is, to our knowledge, the first time it is shown in a general way, using a statistically significant sample, that there is a difference in the viewing angle to the central engine of Seyfert 1’s and Seyfert 2’s, and is an independent confirmation of the Unified Model.

However, if we assume that all the Seyfert 2’s have  $|\phi| > 40^\circ$  we find that NGC4388 would contradict this model, since the analysis of its data requires  $|\phi| \leq 21^\circ$ . We assumed, based on this and the analysis of the  $i$ -distribution of the Seyfert 1’s in our sample, that a galaxy is only recognized as a Seyfert 1 if the jet is seen at an angle  $|\phi| \leq \phi_c$  and the host galaxy inclination is smaller than  $i \leq i_c$ , otherwise it is a Seyfert 2. Comparing the models constructed assuming  $\phi_c = 40^\circ$  and  $i_c = 60^\circ$  with the observed data for the  $60\mu\text{m}$  sample, we see that all permitted regions of the parameter space is acceptable, with a preference for small values of  $\beta_1$  and large values of  $\beta_2$ .

As we discussed in the introduction, the simplest assumption suggests that the accretion disk is fed from gas in the galaxy disk, so we would expect that both disks have the same angular momentum vector. Since jets are supposed to be launched perpendicular to the accretion disk, the expectation would be to see all the jets aligned with the minor axis. However, as shown above, this expectation is contradicted by our results, which clearly shows that the observed distribution of  $\delta$  and  $i$  values can be represented by a homogeneous  $\beta$ -distribution in the  $0^\circ \leq \beta \leq 90^\circ$  range. We explored two main lines to explain the misalignment between the accretion disk axis and the host galaxy disk axis: i) feeding of the accretion disk by aligned inflow from the galaxy disk, with the misalignment of the accretion disk; ii) feeding of the accretion disk by misaligned gas inflow. In the case of aligned inflow, the randomness of the accretion disks could be due to warping of the accretion disk by self-irradiation instability, warping by the Bardeen-Petterson effect, or warping by a misaligned gravitational potential of a nuclear star cluster surrounding the black hole. In the case of misaligned inflow, the randomness of the jets could be due to misaligned minor mergers, capture of individual stars or gas from the nuclear star cluster, or the capture of individual molecular clouds from the host galaxy.

JEP is grateful for continued support from the STScI visitor program. ALK would like to

thank IoA for support under its visitor program. ALK, HRS and JEP would like to acknowledge the Isaac Newton Institute for Mathematical Sciences for support during the programme “The Dynamics of Astrophysical Discs”, where this work started. HRS and ALK would like to acknowledge the hospitality and help from the staff at CTIO, KPNO, VLA and Lick Observatory. We thank La Palma observatory for the service observing of several galaxies in our sample. Alastair Young, Marcella Carollo, Stefi Baum, Paul Hewett, Gerry Gilmore, Blaise Canzian and the referee, Andrew Wilson are gratefully acknowledged for useful comments and discussions during the development of this paper. This work was supported by NASA grants NAGW-3757, AR-5810.01-94A, AR-6389.01-94A and the HST Director Discretionary fund D0001.82223. This research made use of the NASA/IPAC Extragalactic Database (NED), which is operated by the Jap Propulsion Laboratory, Caltech, under contract with NASA. We also used the Digitized Sky Survey, which was produced at the Space telescope Science Institute under U.S. Government grant NAGW-2166. The National Radio Astronomy Observatory is a facility of the National Science Foundation operated under cooperative agreement by Associated Universities, Inc.

### A. Formulae for $P(\delta | \beta_1, \beta_2, i)$

We consider a line of sight at an angle  $i$  to the galactic pole and a model in which jets are uniformly distributed over the galactic hemisphere at galactic latitudes satisfying  $\beta_1 \leq \beta \leq \beta_2$ . We wish to calculate for given values of  $i, \beta_1, \beta_2$  the probability density function (p.d.f.) as a function of  $\delta$ : we denote the fraction of jets with angles in the plane of the sky in the range  $\delta$  to  $\delta + d\delta$  by  $p(\delta|i, \beta_1, \beta_2)d\delta$ . From this we can readily calculate the corresponding cumulative distribution function (c.d.f.):

$$c(\delta|i, \beta_1, \beta_2) = \int_0^\delta p(\delta'|i, \beta_1, \beta_2)d\delta' . \quad (A1)$$

Note that any jet (viewed at given  $i$ ) for which  $\delta$  is in the range  $\delta$  to  $\delta + d\delta$  is constrained to lie between a pair of great circles (angular separation  $d\delta$ ) with pole at  $\beta = i$  (see Figure 2).

We here introduce the variable  $\Phi$  which, for a given great circle (defined by  $(i, \delta)$ ), measures the angular distance along the great circle from its pole.  $\Phi$  is related to  $i, \beta, \delta$  via

$$\sin \Phi = \frac{\cos \beta \sin \delta \sin i - (\sin^2 \beta - \sin^2 i \cos^2 \delta)^{\frac{1}{2}} \cos i}{1 - \sin^2 i \cos^2 \delta} \quad (A2)$$

Each great circle has two intersections (at  $\Phi = \Phi_1^a$  and  $\Phi = \Phi_1^b$ ) with the line of latitude  $\beta = \beta_1$ , and correspondingly two intersections (at  $\Phi = \Phi_2^a$  and  $\Phi = \Phi_2^b$ ) with the line of latitude  $\beta = \beta_2$ .  $\Phi_1^a, \Phi_1^b, \Phi_2^a$  and  $\Phi_2^b$  are readily obtained from A2 with  $\beta$  set equal to  $\beta_1$  and  $\beta_2$  respectively.

Note that, depending on the values of  $i, \beta_1, \beta_2$  there may be a range of angles,  $\delta$ , for which  $p = 0$ . This means that jets with such angles lie on great circles which do not intersect the band of latitudes that are populated with jets in the model. In general, for a line of latitude at  $\beta = b$ ,

all great circles intersect this line if  $i < b$ , but if  $i > b$  intersection occurs only for

$$\delta > \delta_b = \cos^{-1} \left( \frac{\sin b}{\sin i} \right) \quad (A3)$$

We denote the probability density of sources per unit solid angle on the galactic sphere by  $\Sigma(\beta, \theta)$ . Since a complete set of great circles (with  $\delta$  in the range 0 to  $\frac{\pi}{2}$ ) covers an area equal to half the galactic hemisphere, we normalize  $\Sigma$  such that  $\Sigma(\beta, \theta)d\Omega$  is the fraction of sources in half of the galactic hemisphere that are contained in a solid angle  $d\Omega$  centered on  $[\beta, \theta]$ . For a uniform band of jet orientations between  $\beta = \beta_1$  and  $\beta = \beta_2$  we have

$$\begin{aligned} \Sigma &= \frac{1}{\pi(\cos \beta_1 - \cos \beta_2)} && (\beta_1 < \beta < \beta_2) \\ &= 0 && \text{otherwise} \end{aligned} \quad (A4)$$

The fraction of jets, therefore, to be found in a small surface element lying between  $\Phi$  and  $\Phi + d\Phi$ , between the pair of great circles with angles  $\delta$  and  $\delta + d\delta$  is thus  $\Sigma \sin \Phi d\Phi d\delta$ .

Therefore the fraction of jets lying anywhere between this pair of great circles is  $\int \Sigma \sin \Phi d\Phi d\delta$  so that

$$p(\delta|i, \beta_1, \beta_2) = \int \Sigma \sin \Phi d\Phi \quad (A5)$$

In order to derive explicit forms for  $p$ , we distinguish 3 regimes:

i)  $i > \beta_2$

Here great circles fall in 3 categories: a) those that never intercept the band of latitudes populated by jets; b) those that intercept the populated band but not the empty polecap region; and c) those that traverse both the populated band and the empty polecap. In these cases,  $p$  is given respectively by:

$$p = 0 \quad (\text{for } \delta < \delta_{b_2}) \quad (A6a)$$

$$p = \Sigma \left( \cos \Phi_2^a - \cos \Phi_2^b \right) \quad (\text{for } \delta_{b_2} < \delta < \delta_{b_1}) \quad (A6b)$$

$$p = \Sigma \left( \cos \Phi_2^a - \cos \Phi_2^b - \cos \Phi_1^a + \cos \Phi_1^b \right) \quad (\text{for } \delta > \delta_{b_1}). \quad (A6c)$$

where  $\delta_{b_1}$  and  $\delta_{b_2}$  are the values of  $\delta_b$  (A3) for  $b = \beta_1$  and  $b = \beta_2$  respectively.

Substituting for  $\Phi_1^a$ ,  $\Phi_1^b$ ,  $\Phi_2^a$ ,  $\Phi_2^b$  from (A2) we obtain

$$p = 0 \quad (\delta < \delta_{b_2}) \quad (A7a)$$

$$p = \frac{2 \sin \delta \sin i (\sin^2 \beta_2 - \sin^2 i \cos^2 \delta)^{\frac{1}{2}}}{\pi (\cos \beta_1 - \cos \beta_2) (1 - \sin^2 i \cos^2 \delta)}. \quad (\delta_{b_2} < \delta < \delta_{b_1}) \quad (A7b)$$

$$p = \frac{2 \sin \delta \sin i \left( (\sin^2 \beta_2 - \sin^2 i \cos^2 \delta)^{\frac{1}{2}} - (\sin^2 \beta_1 - \sin^2 i \cos^2 \delta)^{\frac{1}{2}} \right)}{\pi (\cos \beta_1 - \cos \beta_2) (1 - \sin^2 i \cos^2 \delta)} \quad (\delta > \delta_{b_1}) \quad (A7c)$$

The corresponding cumulative distribution functions (A1) are then

$$c = 0 \quad (\delta < \delta_{b_2}) \quad (A8a)$$

$$c = \frac{2}{\pi (\cos \beta_1 - \cos \beta_2)} \left[ \frac{\pi}{2} - \sin^{-1} \left( \frac{\cos \delta}{\cos \delta_{b_2}} \right) - \frac{1}{2} \cos \beta_2 \sin^{-1} \Psi_2 \right] \quad (\delta_{b_2} < \delta < \delta_{b_1}) \quad (A8b)$$

$$c = \frac{2}{\pi (\cos \beta_1 - \cos \beta_2)} \left[ \sin^{-1} \left( \frac{\cos \delta}{\cos \delta_{b_1}} \right) + \frac{1}{2} \cos \beta_1 \sin^{-1} \Psi_1 - \sin^{-1} \left( \frac{\cos \delta}{\cos \delta_{b_2}} \right) - \frac{1}{2} \cos \beta_2 \sin^{-1} \Psi_2 \right] \quad (\delta > \delta_{b_1}) \quad (A8c)$$

where

$$\Psi_2 = \frac{2 \cos \beta_2 \left( \frac{\cos \delta}{\cos \delta_{b_2}} \right) \sqrt{1 - \left( \frac{\cos \delta}{\cos \delta_{b_2}} \right)^2}}{1 - \sin^2 i \cos^2 \delta}. \quad (A9a)$$

and

$$\Psi_1 = \frac{2 \cos \beta_1 \left( \frac{\cos \delta}{\cos \delta_{b_1}} \right) \sqrt{1 - \left( \frac{\cos \delta}{\cos \delta_{b_1}} \right)^2}}{1 - \sin^2 i \cos^2 \delta}. \quad (A9b)$$

Note that  $\sin^{-1} \Psi_1$ ,  $\sin^{-1} \Psi_2$  are defined as monotonically increasing functions of  $\delta$  in the range 0 to  $\pi$ .

ii)  $\beta_1 < \beta < \beta_2$

Here the line of sight passes through the populated band of latitudes. Recalling that all great circles intersect the line of longitude  $\beta = \beta_2$ , but that only those with  $\delta > \delta_{b_1}$  intersect the line  $\beta = \beta_1$ , we have

$$p = \Sigma \left( 2 - \left( \cos \Phi_2^a + \cos \Phi_2^b \right) \right) \quad (\delta < \delta_{b_1}) \quad (A10a)$$

$$p = \Sigma \left( 2 - \left( \cos \Phi_2^a + \cos \Phi_2^b \right) - \left( \cos \Phi_1^a - \cos \Phi_1^b \right) \right) \quad (\delta > \delta_{b_1}) \quad (A10b)$$

which can be written

$$p = \frac{2}{\pi (\cos \beta_1 - \cos \beta_2)} \left( 1 - \frac{\cos \beta_2 \cos i}{(1 - \sin^2 i \cos^2 \delta)} \right) \quad (\delta < \delta_{b_1}) \quad (A11a)$$

$$p = \frac{2}{\pi (\cos \beta_1 - \cos \beta_2)} \left( 1 - \frac{\left( \cos \beta_2 \cos i + \sin \delta \sin i \left( \sin^2 \beta_1 - \sin^2 i \cos^2 \delta \right)^{\frac{1}{2}} \right)}{1 - \sin^2 i \cos^2 \delta} \right) \quad (\delta > \delta_{b_1}) \quad (A11b)$$

The corresponding cumulative distributions are:

$$c = \frac{2}{\pi(\cos \beta_1 - \cos \beta_2)} \left( \delta - \frac{1}{2} \cos \beta_2 \sin^{-1} \Psi \right) (\delta < \delta_{b_1}) \quad (A12a)$$

$$c = \frac{2}{\pi(\cos \beta_1 - \cos \beta_2)} \left( \delta - \frac{1}{2} \cos \beta_2 \sin^{-1} \Psi - \frac{\pi}{2} + \sin^{-1} \left( \frac{\cos \delta}{\cos \delta_{b_1}} \right) + \frac{1}{2} \cos \beta_1 \sin^{-1} \Psi_1 \right) (\delta > \delta_{b_1}) \quad (A12b)$$

where  $\Psi_1$  is given by (A9b) and

$$\Psi = \frac{2 \cos i \sin \delta \cos \delta}{1 - \cos^2 \delta \sin^2 i} \quad (A13)$$

Again, both  $\sin^{-1} \Psi_1$  and  $\sin^{-1} \Psi$  are monotonically increasing functions of  $\delta$  in the range 0 to  $\pi$ .

iii)  $i < \beta_1$

In this case, all great circles intercept both the lines  $\beta = \beta_1$  and  $\beta = \beta_2$ . Here

$$p = \Sigma \left( \left( \cos \Phi_1^a + \cos \Phi_1^b \right) - \left( \cos \Phi_2^a + \cos \Phi_2^b \right) \right) \quad (A14)$$

which becomes

$$p = \frac{2 \cos i}{\pi (1 - \sin^2 i \cos^2 \delta)} \quad (A15)$$

so that

$$c = \frac{1}{\pi} \sin^{-1} \left[ \frac{2 \cos i \cos \delta \sin \delta}{1 - \sin^2 i \cos^2 \delta} \right]. \quad (A16)$$

Note that in this regime (where the line of sight passes through the excluded polecap), the probability density function is independent of  $\beta_1$  and  $\beta_2$ .

## B. Formulae for $P(\delta | \beta_1, \beta_2, i)$ in the case when there is information about frontside and backside of the galaxy

We now derive corresponding expressions (see Appendix A for definitions) in the case that we know whether a galaxy is a ‘frontside’ or ‘backside’ source (i.e. whether the jet lies on the short arc of the great circle, length  $|\Phi_1|$ , or the long arc, length  $180 - |\Phi_1|$ ). As before, we distinguish three regimes:

i)  $i > \beta_2$

In this case the ‘frontside’ arc does not intercept the region populated by jets, so all such galaxies must be ‘backside’ sources. The p.d.f. ( $p$ ) and c.d.f. ( $c$ ) for these ‘backside’ sources are given by equations (A6) to (A9).

ii)  $\beta_1 < \beta < \beta_2$

We now denote the surface density of jets by  $\Sigma_f$  and  $\Sigma_b$  for regions of the galactic sphere intercepted by ‘frontside’ and ‘backside’ arcs respectively. We fix  $\Sigma_f$  and  $\Sigma_b$  by appropriate normalization below.

For frontside sources:

$$p = \Sigma_f (1 - \cos \Phi_2^a)$$

which can be written

$$p = \Sigma_f \left( 1 - \frac{\left( \cos \beta_2 \cos i + \sin \delta \sin i (\sin^2 \beta_2 - \sin^2 i \cos^2 \delta)^{\frac{1}{2}} \right)}{1 - \sin^2 i \cos^2 \delta} \right) \quad (B1)$$

The corresponding c.d.f. is given by:

$$c = \Sigma_f \left( \delta - \frac{1}{2} \cos \beta_2 \sin^{-1} \Psi + \sin^{-1} \left( \frac{\cos \delta \sin i}{\sin \beta_2} \right) + \frac{1}{2} \cos \beta_2 \sin^{-1} \Psi_2 - \sin^{-1} \left( \frac{\sin i}{\sin \beta_2} \right) - \frac{1}{2} \cos \beta_2 \sin^{-1} \Psi_2|_0 \right) \quad (B2)$$

where  $\Psi_2$  and  $\Psi$  are given by equations (A9) and (A13) and  $\Psi_2|_0$  is equal to  $\Psi_2$  evaluated at  $\delta = 0$ . Note that as before, both  $\sin^{-1} \Psi_2$  and  $\sin^{-1} \Psi$  are equal to  $\pi$  when  $\delta = \pi/2$ , and are monotonically increasing functions of  $\delta$  for  $\delta$  in the range 0 to  $\pi/2$ . Normalising so that  $c = 1$  when  $\delta = \pi/2$  we have

$$\Sigma_f = \frac{1}{\frac{\pi}{2} - \sin^{-1} \left( \frac{\sin i}{\sin \beta_2} \right) - \frac{1}{2} \cos \beta_2 \sin^{-1} \Psi_2|_0} \quad (B3)$$

For ‘backside’ sources, we need to distinguish between those great circles (with  $\delta <$  and  $> \delta_{b_1}$ ) that do not and do respectively cross the excluded polecap region:

$$p = \Sigma_b (1 - \cos \Phi_2^b) \quad (\delta < \delta_{b_1}) \quad (B4a)$$

$$p = \Sigma_b (1 - \cos \Phi_2^b - (\cos \Phi_1^a - \cos \Phi_1^b)) \quad (\delta > \delta_{b_1}) \quad (B4b)$$

which can be written

$$p = \Sigma_b \left( 1 - \frac{\left( \cos \beta_2 \cos i - \sin \delta \sin i (\sin^2 \beta_2 - \sin^2 i \cos^2 \delta)^{\frac{1}{2}} \right)}{1 - \sin^2 i \cos^2 \delta} \right) \quad (\delta < \delta_{b_1}) \quad (B5a)$$

$$p = \Sigma_b \left( 1 - \frac{\left( \cos \beta_2 \cos i - \sin \delta \sin i \left( (\sin^2 \beta_2 - \sin^2 i \cos^2 \delta)^{\frac{1}{2}} - (\sin^2 \beta_1 - \sin^2 i \cos^2 \delta)^{\frac{1}{2}} \right) \right)}{1 - \sin^2 i \cos^2 \delta} \right) \quad (\delta > \delta_{b_1}) \quad (B5b)$$

The corresponding c.d.f. are given by:

$$c = \Sigma_b \left[ \delta - \frac{1}{2} \cos \beta_2 \sin^{-1} \Psi - \sin^{-1} \left( \frac{\cos \delta \sin i}{\sin \beta_2} \right) - \frac{1}{2} \cos \beta_2 \sin^{-1} \Psi_2 + \sin^{-1} \left( \frac{\sin i}{\sin \beta_2} \right) + \frac{1}{2} \cos \beta_2 \sin^{-1} \Psi_2|_0 \right] \quad (\delta < \delta_{b_1}) \quad (B6a)$$

$$c = \Sigma_b \left[ \delta - \pi - \frac{1}{2} \cos \beta_2 \sin^{-1} \Psi - \sin^{-1} \left( \frac{\cos \delta \sin i}{\sin \beta_2} \right) - \frac{1}{2} \cos \beta_2 \sin^{-1} \Psi_2 + \sin^{-1} \left( \frac{\sin i}{\sin \beta_2} \right) + \frac{1}{2} \cos \beta_2 \sin^{-1} \Psi_2|_0 + 2 \sin^{-1} \left( \frac{\cos \delta \sin i}{\sin \beta_1} \right) + \cos \beta_1 \sin^{-1} \Psi_1 \right] \quad (\delta > \delta_{b_1}) \quad (B6b)$$

Normalising so that  $c = 1$  for  $\delta = \pi/2$  we have

$$\Sigma_b = \frac{1}{\pi (\cos \beta_1 - \cos \beta_2) - \frac{\pi}{2} + \sin^{-1} \left( \frac{\sin i}{\sin \beta_2} \right) + \frac{1}{2} \cos \beta_2 \sin^{-1} \Psi_2|_0} \quad (B7)$$

iii)  $i < \beta_1$

For frontside galaxies:

$$p = \Sigma_f (\cos \Phi_1^a - \cos \Phi_2^a)$$

which may be written:

$$p = \Sigma_f \left( \frac{(\cos \beta_1 - \cos \beta_2) \cos i - \sin \delta \sin i \left( (\sin^2 \beta_2 - \sin^2 i \cos^2 \delta)^{\frac{1}{2}} - (\sin^2 \beta_1 - \sin^2 i \cos^2 \delta)^{\frac{1}{2}} \right)}{1 - \sin^2 i \cos^2 \delta} \right) \quad (B8)$$

with a corresponding cumulative distribution

$$c = \Sigma_f \left[ \frac{1}{2} (\cos \beta_1 - \cos \beta_2) \sin^{-1} \Psi + \sin^{-1} \left( \frac{\cos \delta \sin i}{\sin \beta_2} \right) + \frac{1}{2} \cos \beta_2 \sin^{-1} \Psi_2 - \sin^{-1} \left( \frac{\sin i}{\sin \beta_2} \right) \right. \\ \left. - \frac{1}{2} \cos \beta_2 \sin^{-1} \Psi_2|_0 - \sin^{-1} \left( \frac{\cos \delta \sin i}{\sin \beta_1} \right) - \frac{1}{2} \cos \beta_1 \sin^{-1} \Psi_1 + \sin^{-1} \left( \frac{\sin i}{\sin \beta_1} \right) \right. \\ \left. + \frac{1}{2} \cos \beta_1 \sin^{-1} \Psi_1|_0 \right] \quad (B9)$$

As before  $\sin^{-1} \Psi, \sin^{-1} \Psi_2$  and  $\sin^{-1} \Psi_1$  are each equal to  $\pi$  for  $\delta = \frac{\pi}{2}$  and are monotonically increasing functions of  $\delta$ .  $\Psi_1|_0$  is equal to  $\Psi_1$  evaluated at  $\delta = 0$ . Normalising so that  $c = 1$  for  $\delta = \frac{\pi}{2}$ :

$$\Sigma_f = \frac{1}{\sin^{-1} \left( \frac{\sin i}{\sin \beta_1} \right) - \sin^{-1} \left( \frac{\sin i}{\sin \beta_2} \right) + \frac{1}{2} \cos \beta_1 \sin^{-1} \Psi_1|_0 - \frac{1}{2} \cos \beta_2 \sin^{-1} \Psi_2|_0} \quad (B10)$$

For backside galaxies:

$$p = \Sigma_b \left( \cos \Phi_1^b - \cos \Phi_2^b \right)$$

which may be written:

$$p = \Sigma_b \left( \frac{(\cos \beta_1 - \cos \beta_2) \cos i + \sin \delta \sin i \left( (\sin^2 \beta_2 - \sin^2 i \cos^2 \delta)^{\frac{1}{2}} - (\sin^2 \beta_1 - \sin^2 i \cos^2 \delta)^{\frac{1}{2}} \right)}{1 - \sin^2 i \cos^2 \delta} \right) \quad (B11)$$

with a corresponding cumulative distribution

$$c = \Sigma_b \left[ \frac{1}{2} (\cos \beta_1 - \cos \beta_2) \sin^{-1} \Psi - \sin^{-1} \left( \frac{\cos \delta \sin i}{\sin \beta_2} \right) - \frac{1}{2} \cos \beta_2 \sin^{-1} \Psi_2 + \sin^{-1} \left( \frac{\sin i}{\sin \beta_2} \right) \right. \\ \left. + \frac{1}{2} \cos \beta_2 \sin^{-1} \Psi_2|_0 + \sin^{-1} \left( \frac{\cos \delta \sin i}{\sin \beta_1} \right) + \frac{1}{2} \cos \beta_1 \sin^{-1} \Psi_1 - \sin^{-1} \left( \frac{\sin i}{\sin \beta_1} \right) \right. \\ \left. - \frac{1}{2} \cos \beta_1 \sin^{-1} \Psi_1|_0 \right] \quad (B12)$$

Normalisation ( $c = 1$  for  $\delta = \frac{\pi}{2}$ ) then yields:

$$\Sigma_b = \frac{1}{\pi (\cos \beta_1 - \cos \beta_2) - \sin^{-1} \left( \frac{\sin i}{\sin \beta_1} \right) + \sin^{-1} \left( \frac{\sin i}{\sin \beta_2} \right) - \frac{1}{2} \cos \beta_1 \sin^{-1} \Psi_1|_0 + \frac{1}{2} \cos \beta_2 \sin^{-1} \Psi_2|_0} \quad (B13)$$

## REFERENCES

- Antonucci, R. 1999, in High Energy Processes in Accreting Black Holes, ASP Conference Series 161, ed. J. Poutanen and R. Svensson 1999, p. 193
- Bardeen, J.M., & Petterson, J.A., 1975. *ApJ*, 195, L65
- Barnes, J.E., & Hernquist, L., 1992. *ARA&A*, 30, 70
- Barnes, J.E., & Hernquist, L. 1996. *ApJ*, 471, 115
- Baum, S.A., O’Dea, C.P., de Bruyn, A.G., & Pedlar, A., 1993, *ApJ*, 419, 553
- Brindle, C., Hough, J. H., Bailey, J. A., Axon, D. J., Ward, M. J., Sparks, W. B. & McLean, I. S. 1990, *MNRAS*, 244, 577
- Byrd, G.G., Valtonen, M.J., Sundelius, B., & Valtaoja, 1986. *A&A*, 166, 75
- Capetti, A., Axon, D.J., Machetto, F.D., Sparks, W.B., & Boksenberg, A., 1996. *ApJ*, 469, 554
- Carollo, C.M., 1999. *ApJ*, 523, 566
- Carollo, C.M., & Stiavelli, M., 1998. *AJ*, 115, 2306
- Carollo, C.M., Stiavelli, M., De Zeeuw, P.T., & Mack, J., 1997. *AJ*, 114, 2366
- Chatzichristou, E. T. 1999, PhD Thesis, University of Leiden
- Clarke, C., Kinney, A.L., & Pringle, J.E. 1998, *ApJ*, 495, 189
- Colina, L., Vargas, M.L.G., Delgado, R.M.G., Mas-Hesse, J.M., Perez, E., Alberdi, A., & Krabbe, A., 1997. *ApJ*, 488, L71
- Davidge, T.J., Rigaut, F., Doyon, R., & Crampton, D., 1997a. *AJ*, 113, 2094
- Davidge, T.J., Simons, D.A., Rigaut, F., Doyon, R., & Crampton, D., 1997b. *AJ*, 114, 2586
- deGrijp, M.H.K., Keel W.C., Miley, G.K., Goudfrooij, P. & Lub, J., 1992, *AAS*, 96, 389
- deGrijp, M.H.K., Miley, G.K., & Lub, J., 1987, *AAS*, 70, 95
- De Koff, S., Best, P., Baum, S.A., Sparks, W., Röttgering, H., Miley, G., Golombek, D., & Macchetto, F., 1999. *ApJ*, in preparation
- De Robertis, M.M., Hayhoe, K., & Yee, H.K.C., 1998a. *ApJS*, 115, 163
- De Robertis, M.M., Yee, H.K.C., & Hayhoe, K., 1998b. *ApJ*, 496, 93
- Dultzin-Hacyan, D., Krongold, Y., Fuentes-Guridi, I., & Marziani, P. 1999, *ApJ*, 513, L111
- Efstathiou, A., Rowan-Robinson, M. 1995, *MNRAS*, 273, 649
- Faber, S.M., Tremaine, S., Ajhar, E.A., Byun, Y.-I., Dressler, A., Gebhardt, K., Grillmair, C., Kormendy, J., Lauer, T.R., Richstone, D., 1997. *AJ*, 114, 1771
- Frank, J., & Rees, M.J., 1976. *MNRAS*, 176, 633
- Galletta, G., 1996. In "Barred Galaxies", IAU Colloquium 117, PASP Conf Series, 91, 429

- Gallimore, J. F., Baum, S. A., O’Dea, C. P., Pedlar, A. & Brinks, E. 1999, ApJ, 524, 684
- Gallimore, J. F., Baum, S. A., O’Dea, C. P. 1996, ApJ, 464, 198
- García-Burillo, S., Sempere, M.J., & Bettoni, D., 1998. ApJ, 502, 325
- Gebhardt, K., Richstone, D., Ajhar, E.A., Lauer, T.R., Byun, Y.-I., Kormendy, J., Dressler, A., Faber, S.M., Grillmair, C., Tremaine, S., 1996. AJ, 112, 105
- Genzel, R., Thatte, N., Krabbe, A., Kroker, H., Tacconi-Garman, L.E., 1996. ApJ, 472, 153
- Hernquist, L., & Mihos, C.J., 1996. AJ, 471, 115
- Ho, L. C., Filippenko, A. V. & Sargent, W.L.W. 1997, ApJ, 487, 591
- Hubble, E. 1926, ApJ, 64, 321
- Keel, W. C. 1980, AJ, 85, 198
- Keel, W.C., deGrijp, M.H.K., Miley, G.K. & Zheng, W., 1994, A&A, 283, 791
- Kuijken, K., Fisher, D., & Merrifield, M.R., 1996. MNRAS, 283, 543
- Kumar, S., & Pringle, J.E., 1985. MNRAS, 213, 435
- Lawrence, A. & Elvis, M. 1982, ApJ, 256, 410
- Magorrian, J., & Tremaine, S., 1999. MNRAS, 309, 447
- Maiolino, R. & Rieke, G. H. 1995, ApJ, 454, 95
- Malkan, M.A., Gorjan, V., & Tam, R., 1998. ApJS, 117,25
- Maloney, P.R., Begelman, M.C. & Pringle, J.E., 1996, ApJ, 472, 582
- Martel, A.R. et al. 1999, ApJS, 122, 81
- Merritt, D., & Quinlan, G.D., 1998. ApJ, 498, 625
- Morganti, R. Tsvetanov, Z. I., Gallimore, J. & Allen, M. G. 1999, A&AS, 137, 457
- Mulchaey, J.S., & Regan, M.W., 1997. ApJ, 482, L135
- Nagar, N., & Wilson, A.S. 1999, ApJ, 516, 97
- Nagar, N., Wilson, A.S., Mulchaey, J.S. & Gallimore, J.F. 1999, ApJS, 120, 209
- Natarajan, P., & Pringle, J.E., 1998. ApJ, 506, L97
- Ogilvie, G.I., 1999. MNRAS, 304, 557
- Osterbrock, D. E. & Martel, A. 1993, ApJ, 414, 552
- Osterbrock, D. E. & Shaw, R. A. 1988, ApJ, 327, 89
- Ozernoy, L.M., Genzel, R., Usov, V.V., 1997. MNRAS, 288, 237
- Papaloizou, J.C.B., & Pringle, J.E., 1983. MNRAS, 202, 1181
- Pedlar, A., Fernandez, B., Hamilton, N.G., Redman, M.P., & Dewdney, R.E. 1998, MNRAS, 300, 1071

- Pier, E.A., & Krolik, J.H., 1992, ApJ, 401, 99
- Pringle, J.E., 1996. MNRAS, 281, 357
- Pringle, J.E., 1997. MNRAS, 292, 136
- Roy, A.L. et al. 2000, in Perspectives in Radio Astronomy: Imperatives at cm and m Wavelengths (Dwingeloo: NFRA), Eds: M.P. van Haarlem & J.M. van der Hulst
- Rubin, V., 1994. AJ, 108, 456
- Sakamoto, K., Scoville, N.Z., Yun, M.S., Crosas, M., Genzel, R., Tacconi, L.J., 1999. ApJ, 514, 68
- Scheuer, P.A.G., & Feiler, R., 1996. MNRAS, 282, 291
- Schmitt, H. R. et al. 2000, in preparation
- Schmitt, H. R. & Kinney, A. L. 1996, ApJ, 463, 623
- Schmitt, H. R. & Kinney, A. L. 2000, ApJS, in press
- Schmitt, H.R., Kinney, A.L., Storchi-Bergmann, T., & Antonucci R., 1997, ApJ, 477, 623
- Sellwood, J.A., & Moore, 1999. ApJ, 510, 125
- Shlosman, I., Begelman, M.C., & Frank, J., 1990. Nature, 345, 679
- Shlosman, I., Frank, J., & Begelman, M.C., 1989. Nature, 338, 45
- Sil'chenko, O.K., 1999. ALett, 25, 140
- Sil'chenko, O.K., Vlasjuk, V.V., Burenkov, A.N., 1997. A&A, 326, 941
- Sil'chenko, O.K., Burenkov, A.N., Vlasjuk, V.V., 1998. A&A, 337, 349
- Simpson, C., Wilson, A.S., Bower, G., Heckamn, T.M., Krolik, J.H., & Miley, G.K., 1997. ApJ, 474, 121
- Syer, D., & Ulmer, A., 1999. MNRAS, 306, 35
- Stark, A.A., & Binney, J., 1994. ApJ, 426, L31
- Taniguchi, Y. 1999, ApJ, 524, 65
- Thakar, A.R., & Ryden, B.S., 1998. ApJ, 506, 93
- Thakar, A.R., Ryden, B.S., Jore, K.P., & Broeils, A.H., 1997. ApJ, 479, 702
- Thronson, H.A., Hereld, M., Majewski, S., Greenhouse, M., Johnson, P., Spillar, E., Woodward, C.E., Harper, D.A., & Rauscher, B.J., 1989. ApJ, 343, 158
- Tremaine, S., 1995. AJ, 110, 628
- Ulvestad J.S. & Wilson A.S., 1984 ApJ 285, 439.
- Ulvestad, J.S., Wrobel, J.M., Roy, A.L., Wilson, A.S., Falcke, H., & Krichbaum, T.P. 1999, ApJ, 517, L81
- Van der Marel, R.P., 1999. AJ, 117, 744

Van Dokkum, P.G., & Franx, M., 1995. *AJ*, 110, 2027

Velázquez. V., & White, S.D.M., 1999. *MNRAS*, 254, 270

Wilson, A. S. & Colbert, E. J. M. 1995, *ApJ*, 438, 62

Zaritsky, D., Smith, R., Frenk, C.S., & White, S.D.M., 1997. *ApJ*, 478, L53

Zasov, A. V. & Sil'chenko, O. K. 1997, *AR*, 41, 734

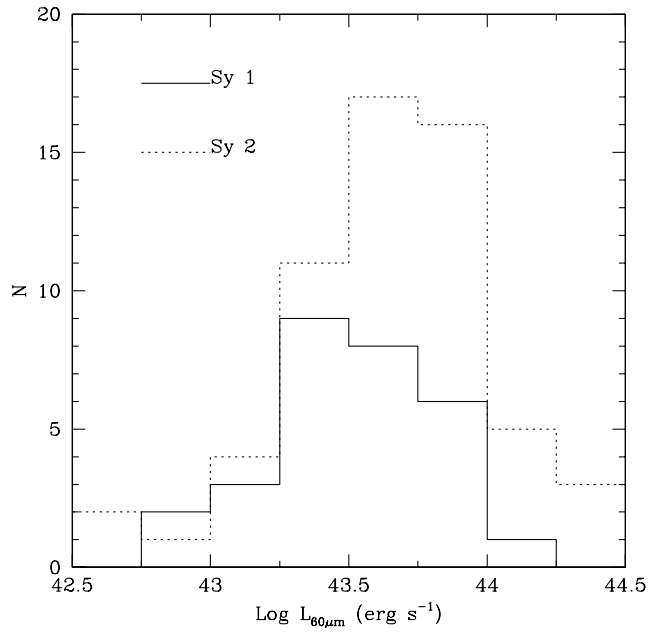


Fig. 1.— Histogram of  $60\mu\text{m}$  luminosities for the  $60\mu\text{m}$  sample. Seyfert 1's are represented by the solid line and Seyfert 2's by the dotted line.

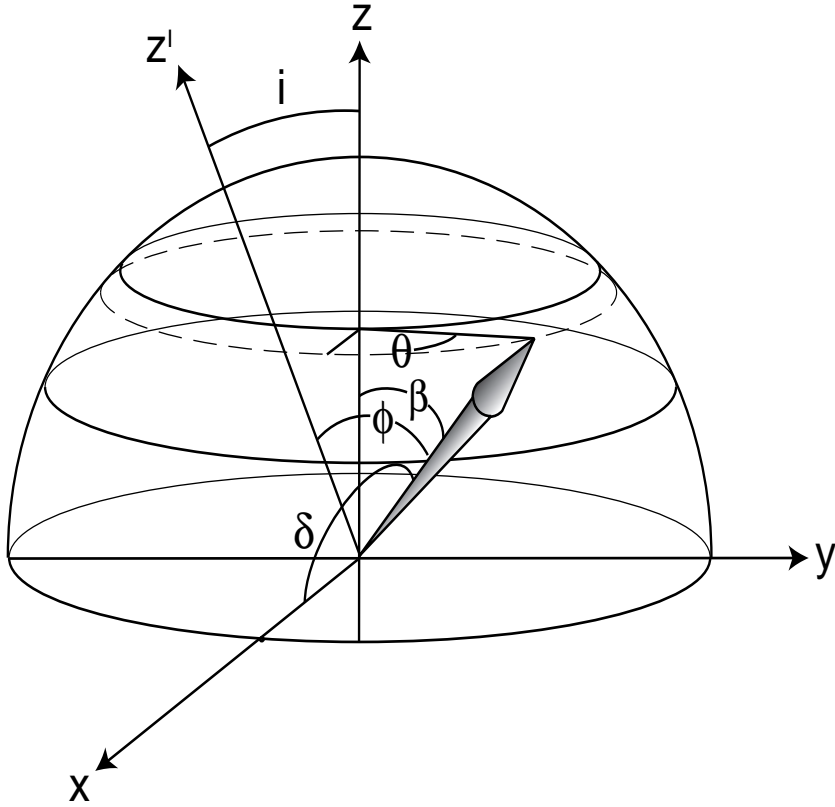


Fig. 2.— The galaxy lies in the  $XY$  plane, with coordinates placed so that the apparent major axis is the  $X$  axis and the galaxy axis is  $Z$ . The line of sight  $Z'$ , designed by the vector  $\mathbf{k}_s$ , is in the plane of the paper. The angle of inclination is  $i$ . The PA between the apparent major axis of the galaxy and the radio jet projected onto the sky plane is  $\delta$ . The radio jet, whose vector is given as  $\mathbf{k}_j$ , is designated by an arrow. The angle between the radio jet and the galaxy axis is  $\beta$ . The angle between the line of sight and the radio axis, commonly referred to as the opening angle of the active galaxy, is  $\phi$ . For an accretion disk perpendicular to the jet,  $\phi = \pm i_{\text{disk}}$ .

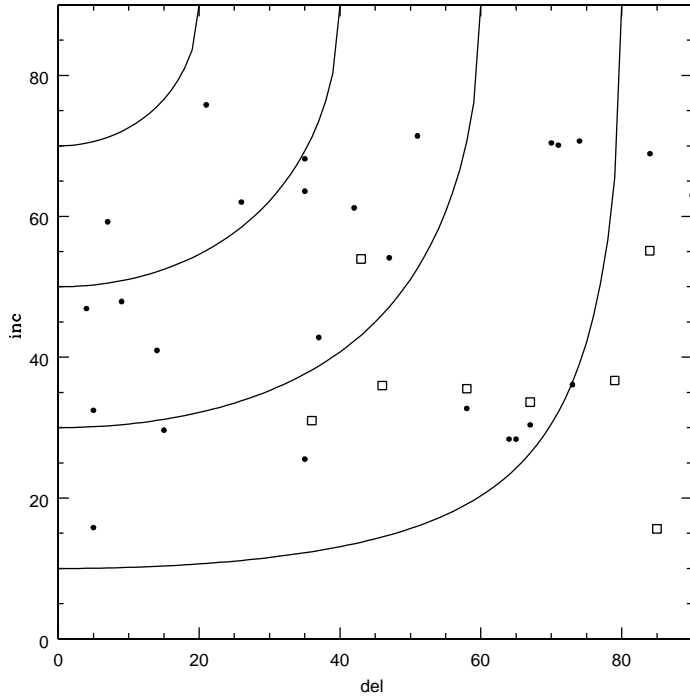
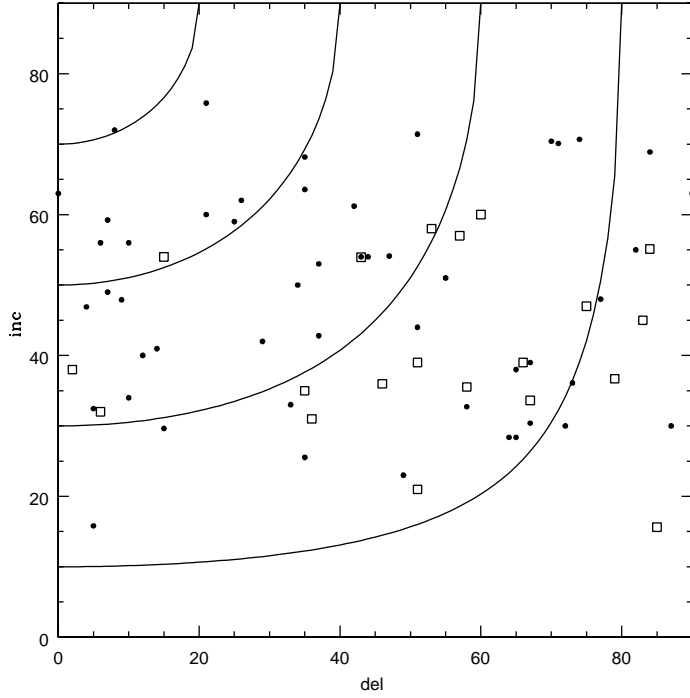


Fig. 3.— a-top) Distribution of observed  $\delta$  and  $i$  values for the total sample (serendipitous +  $60\mu\text{m}$  sources); b-bottom)  $60\mu\text{m}$  sample only. Seyfert 1's are represented by open squares and Seyfert 2's by filled circles. The solid lines represent the contours of constant  $\beta_{min} = 10^\circ, 30^\circ, 50^\circ$  and  $70^\circ$ , from bottom to top, respectively, calculated using Equation 8.

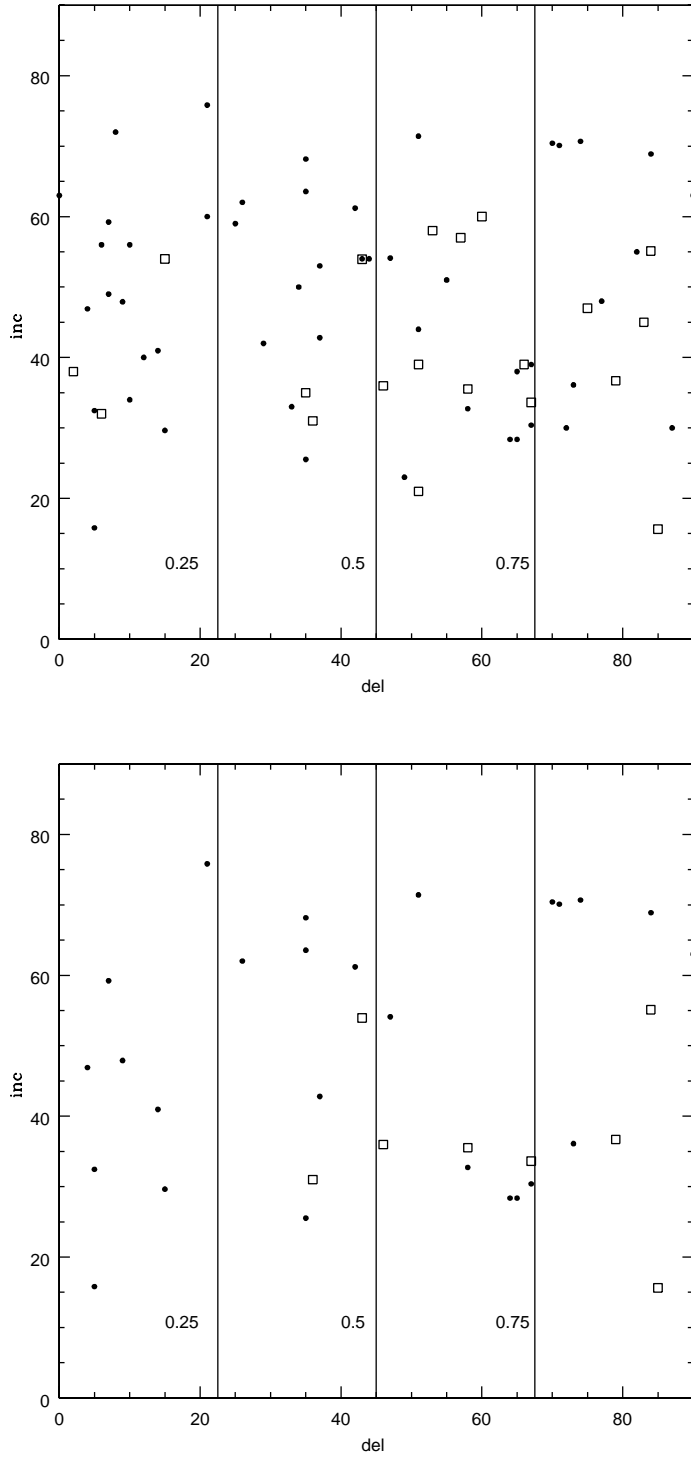


Fig. 4.— Same as Figure 3 for; a-top) the total sample; b-bottom) the 60 $\mu$ m sample. The solid lines represent the quartiles (indicated beside the lines) calculated assuming a uniform  $\beta$ -distribution from  $\beta_1 = 0^\circ$  to  $\beta_2 = 90^\circ$  and not differentiating between Seyfert 1's and Seyfert 2's. The KS test shows that the total sample is consistent with the homogeneous distribution model at the 81% level, while the agreement is at the 67% level for the 60 $\mu$ m sample.

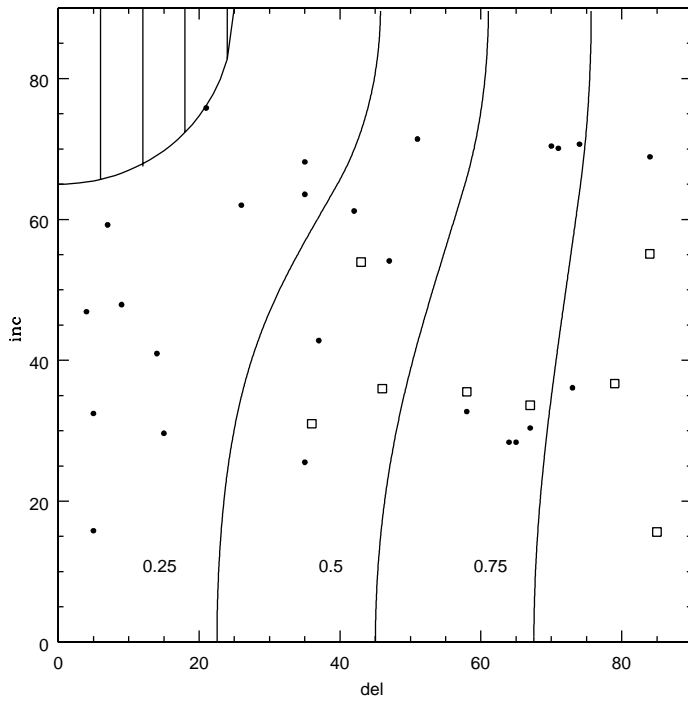


Fig. 5.— The observed  $\delta$  and  $i$  values of the  $60\mu\text{m}$  sample compared with the quartiles (solid lines) calculated assuming a uniform polecap  $\beta$ -distribution, from  $\beta_1 = 0^\circ$  to  $\beta_2 = 65^\circ$  and not differentiating between Seyfert 1'a and Seyfert 2's. The hatched area corresponds to the parameter space excluded by the models. Symbols as in Figure 3. The KS test indicates that the data are consistent with the model at the 69% level.

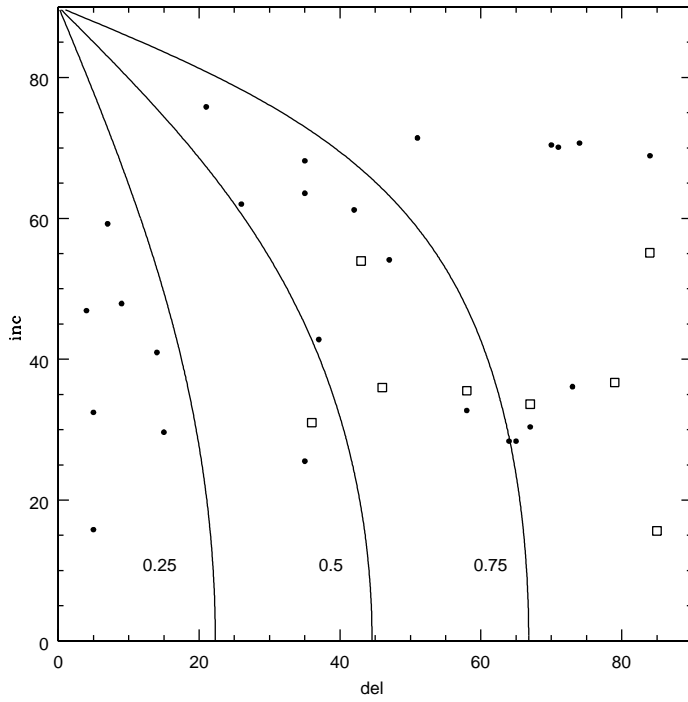


Fig. 6.— The observed  $\delta$  and  $i$  values of the  $60\mu\text{m}$  sample compared with the quartiles (solid lines) calculated assuming the jets are in an equatorial ring,  $\beta_1 = \beta_2 = 90^\circ$ , and not differentiating between Seyfert 1's and Seyfert 2's. The KS test shows that the data are consistent with the model only at the 0.8% level. Symbols as in Figure 3.

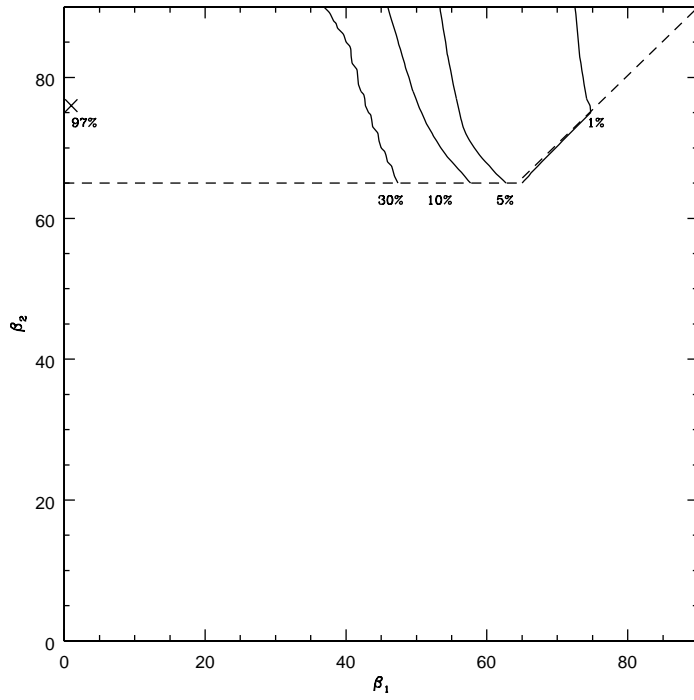
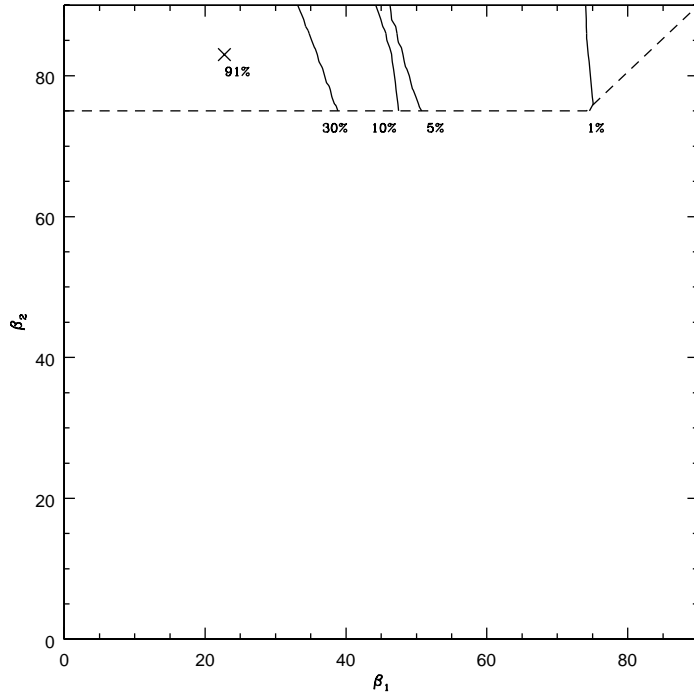


Fig. 7.— Probability contours obtained applying the KS test to the models of uniformly distributed jets over the band  $\beta_1 \leq \beta \leq \beta_2$ , where  $\beta_1 \leq \beta_2$ , and not distinguishing between Seyfert 1's and 2's. a-top) total sample, and b-bottom) the  $60\mu\text{m}$  sample in the.

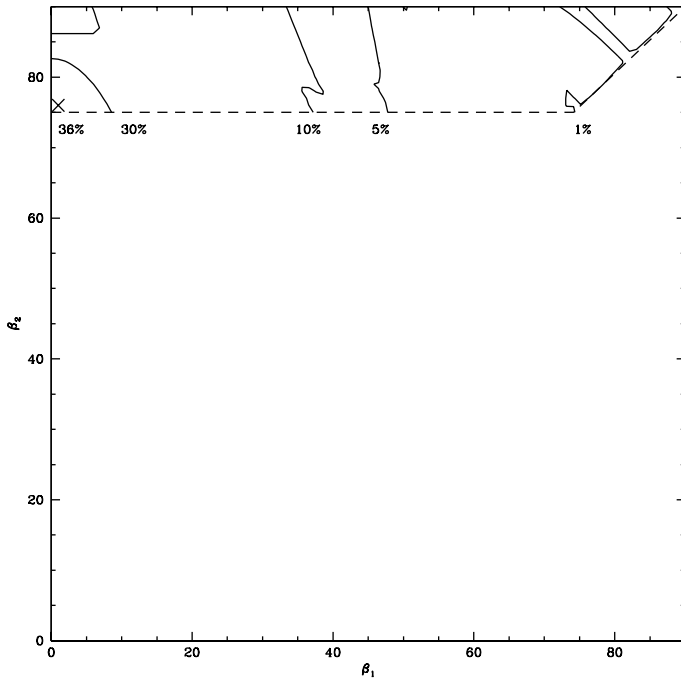


Fig. 8.— Same as Figure 7 for the  $60\mu\text{m}$  sample only, but using the information about near and far side of the galaxy. The acceptability level of the models is reduced in comparison to Figure 7b.

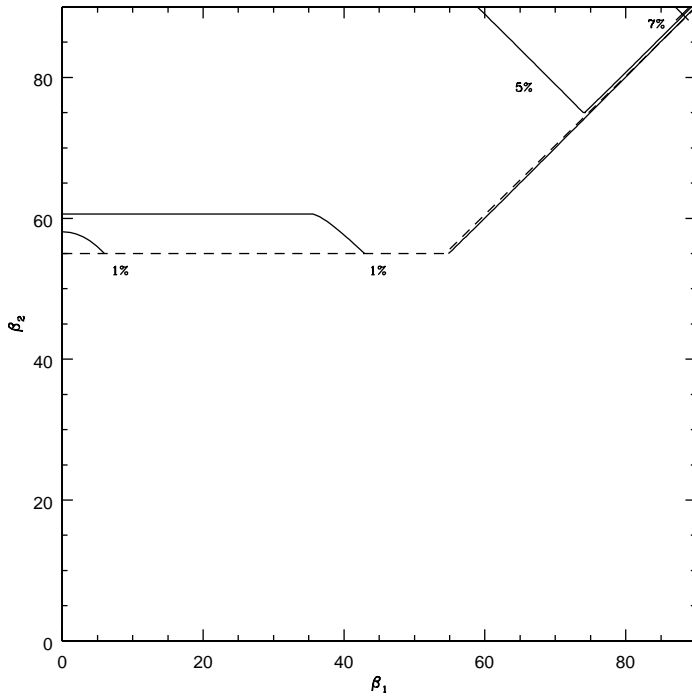
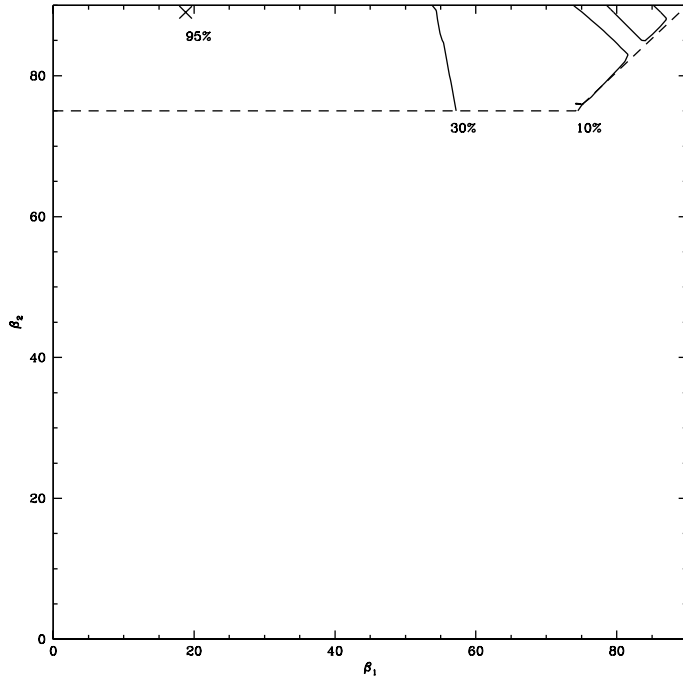


Fig. 9.— Same as Figure 8 but: a-top) distinguishing between Seyfert 2's, and b-bottom) Seyfert 1's. Almost all the permitted parameter space region is accepted for Seyfert 2's, but the maximum acceptability is only 7% for Seyfert 1's.

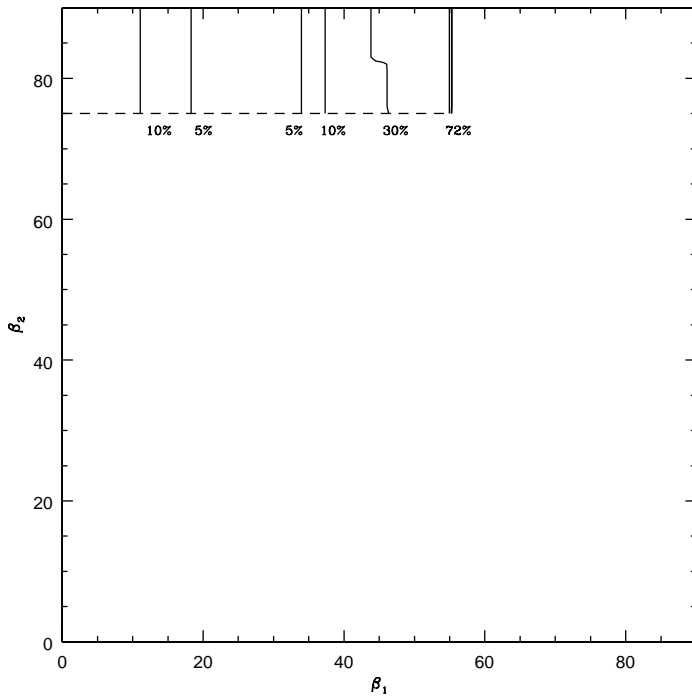


Fig. 10.— Same as Figure 9b, only the Seyfert 1's, but imposing a viewing restriction. That is, a galaxy is only recognized as a Seyfert 1 if the angle between the jet and the line of sight ( $\phi$ ) is smaller than a given value  $\phi_c$ , which we assumed to be equal to  $40^\circ$ .

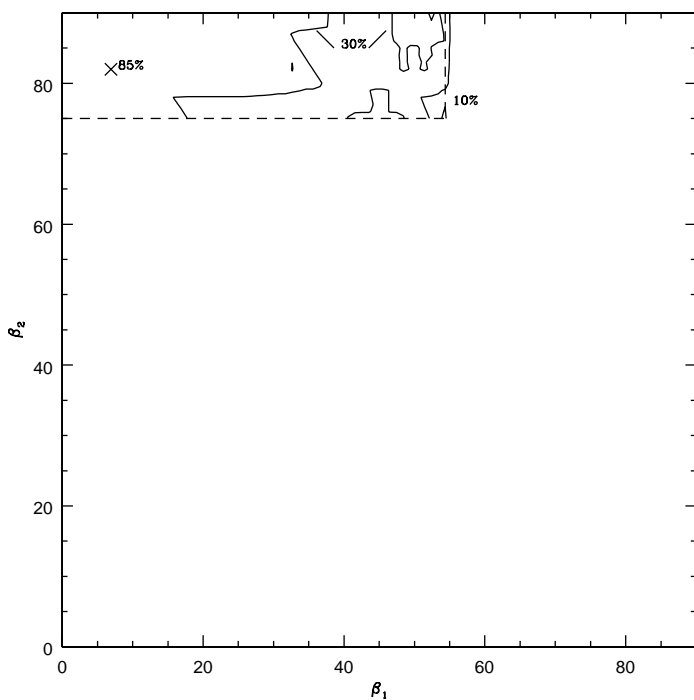


Fig. 11.— Same as Figure 8, using both Seyfert 1’s and 2’s. Here we impose that the galaxy is only recognized as a Seyfert 1 if  $|\phi| < \phi_c$  and if the host galaxy has a small inclination  $i < i_c$ , otherwise the galaxy is classified as a Seyfert 2. We used  $\phi_c = 40^\circ$  and  $i_c = 60^\circ$ .

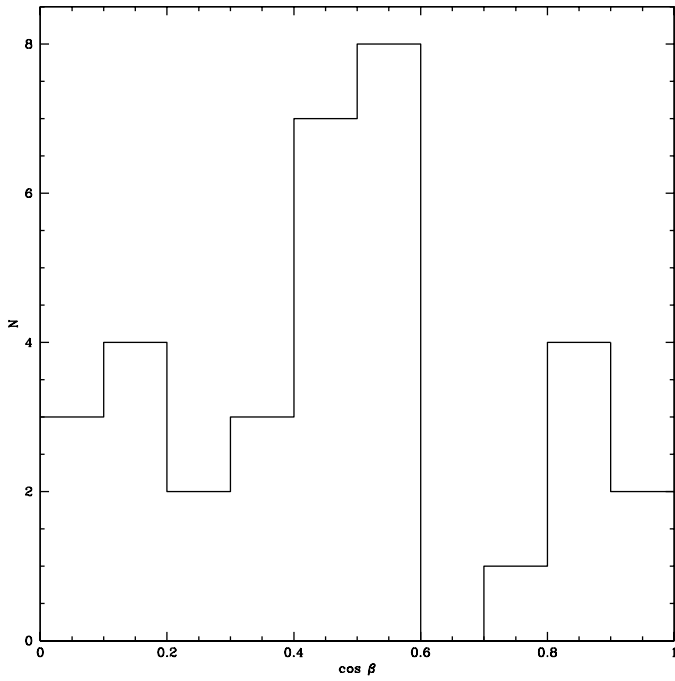


Fig. 12.— The  $\beta$ -distribution obtained making the extreme assumption that all galaxies in the  $60\mu\text{m}$  sample have  $\text{phi}=90$ .

TABLE 1. 60 $\mu$ m Sample Properties

Number	Name	Type	$V_{rad}$ (km s $^{-1}$ )	$L_{60\mu m}$ (erg s $^{-1}$ )	$F_{3.6cm}$ (mJy)	$L_{3.6cm}$ (W Hz $^{-1}$ )	Radio Extent at 3.6cm (pc)	Comments
16	MRK 348	2	4540	43.52	345.6	23.18	33	
24	TOL 0109-38	2	3496	43.38	13.1	21.53	330	
26	MRK 1	2	4780	43.81	11.1	21.73	31	u
27	MRK 359	1	5012	43.37	0.5	20.43	170	
33	MRK 573	2	5174	43.56	1.8	21.01	1003	
37	IRAS 01475-0740	2	5306	43.54	135.4	22.91	34	u
41	ESO 153-G20	2	5917	43.52	—	—	—	
47	MRK 1040	1	4927	43.88	1.1	20.76	32	u
52	ESO 355-G25	2	5039	43.59	—	—	—	
53	UGC 2024	2	6714	44.12	0.7	20.83	43	u
57	NGC 1068	2	1136	44.41	762.4	22.32	745	
67	MCG -02-08-039	2	8874	43.69	2.0	21.53	57	u
68	UGC 2514	1	3957	43.11	0.6	20.30	69	
75	IRAS 03106-0254	2	8154	43.89	10.8	22.18	854	
78	IRAS 03125+0119	2	7200	43.67	8.8	21.99	47	u
83	MRK 607	2	2716	43.27	1.3	20.31	20	u
85	ESO 116-G18	2	5546	43.64	—	—	—	
141	IRAS 04385-0828	2	4527	43.81	7.5	21.52	29	u
154	IRAS 04502-0254	2	4737	43.34	0.4	20.28	107	
156	IRAS 04507+0358	2	8811	43.74	0.8	21.12	205	
157	ESO 33-G02	2	5426	43.34	—	—	—	
174	MCG -05-13-017	1	3790	43.31	2.5	20.88	24	u
196	MRK 3	2	4050	43.85	79.0	22.44	375	
203	UGC 3478	1	3828	43.38	1.4	20.64	25	u
209	MRK 6	1	5537	43.63	30.0	22.29	437	
213	FAIRALL 265	1	8844	43.81	—	—	—	
225	MRK 79	1	6652	43.85	2.9	21.44	1255	
227	MRK 10	1	8785	43.85	0.3	20.69	57	u
233	UGC 4155	1	7645	43.83	2.4	21.48	49	u
236	MRK 622	2	6964	43.85	1.7	21.24	110	
244	ESO 18-G09	2	5341	43.60	—	—	—	
253	MCG -01-24-012	2	5892	43.41	8.9	21.82	133	
260	MRK 1239	1	5974	43.73	7.9	21.78	53	u
272	NGC 3393	2	4107	43.50	10.7	21.59	683	
278	NGC 3516	1	2649	43.15	4.1	20.79	18	
281	IRAS 11215-2806	2	4047	43.01	10.8	21.58	403	
282	MCG -05-27-013	2	7162	43.53	4.7	21.71	1530	
283	MRK 176	2	8346	43.69	6.3	21.97	135	interacting
286	NGC 3783	1	2550	43.42	7.7	21.03	17	u
292	MRK 766	1	3876	43.79	8.6	21.44	67	
293	NGC 4388	2	2524	43.84	9.4	21.11	2940	
299	NGC 4507	2	3538	43.73	—	—	—	
301	NGC 4593	1	2698	43.23	2.1	20.51	17	u
302	TOL 1238-364	2	3285	43.87	—	—	—	
306	NGC 4704	2	8134	44.09	0.8	21.05	53	u
309	MCG -02-33-034	1	4386	43.35	1.2	20.69	28	u interacting
310	ESO 323-G32	2	4796	43.34	—	—	—	
313	MCG -04-31-030	2	2957	43.34	6.5	21.08	478	
314	IRAS 13059-2407	2	4175	43.42	10.4	21.59	27	u
317	MCG -03-34-064	2	5152	44.16	54.1	22.49	278	
322	ESO 383-G18	2	3837	43.01	1.7	20.73	107	
324	MCG -6-30-15	1	2323	42.77	0.9	20.01	110	u
329	NGC 5347	2	2335	42.96	1.6	20.27	15	u
340	IRAS 14082+1347	2	4836	43.96	3.2	21.2	53	
341	NGC 5506	2	1753	43.47	95.0	21.79	302	
344	NGC 5548	1	5149	43.48	3.1	21.24	44	interacting
349	IRAS 14317-3237	2	7615	43.76	1.9	21.37	286	
354	IRAS 14434+2714	2	8814	43.81	8.8	22.16	120	u
369	UGC 9826	1	8754	43.59	0.2	20.51	57	u
377	UGC 9944	2	7354	43.91	5.9	21.83	3430	
383	IRAS 15480-0344	2	9084	44.02	11.2	22.29	59	u
409	IRAS 16288+3929	2	9091	43.78	4.8	21.93	59	u
418	IRAS 16382-0613	2	8317	43.81	2.1	21.49	54	u
445	UGC 10889	2	8424	43.72	1.1	21.22	54	u
447	MCG +03-45-003	2	7292	43.60	0.3	20.53	47	u
471	FAIRALL 49	2	6065	44.09	—	—	—	
473	FAIRALL 51	1	4255	43.56	—	—	—	
497	ESO 143-G09	1	4462	43.33	—	—	—	
501	FAIRALL 341	2	4887	43.32	—	—	—	
510	UGC 11630	2	3657	43.25	0.4	20.06	24	u

TABLE 1. (continued)

Number	Name	Type	$V_{rad}$ ( $\text{km s}^{-1}$ )	$L_{60\mu m}$ ( $\text{erg s}^{-1}$ )	$F_{3.6cm}$ (mJy)	$L_{3.6cm}$ ( $\text{W Hz}^{-1}$ )	Radio Extent at 3.6cm (pc)	Comments
512	PKS 2048-57	2	3402	43.84	229.1	22.75	924	
530	NGC 7213	1	1792	42.93	187.9	22.11	12	u
537	MRK 915	1	7230	43.48	14.7	22.21	47	u
538	UGC 12138	1	7375	43.72	1.9	21.34	81	u
540	AKN 564	1	7195	43.67	7.0	21.89	316	
549	UGC 12348	2	7585	43.97	1.1	21.13	118	u
555	NGC 7674	2	8713	44.64	39.8	22.81	422	
590	MRK 590	1	7910	43.49	3.2	21.63	51	u
594	MRK 1058	2	5138	43.19	0.2	20.05	33	u
602	NGC 1386	2	868	42.61	10.8	20.24	20	
615	MCG +8-11-11	1	6141	44.06	24.4	22.29	1230	
627	MRK 705	1	8658	43.65	2.0	21.50	56	u
634	NGC 3281	2	3200	43.85	17.0	21.57	60	
638	UGC 6100	2	8778	43.65	0.8	21.12	57	u
665	NGC 4941	2	1108	42.26	4.0	20.02	15	
703	UGC 10683B	1	9234	43.61	0.6	21.04	60	u interacting
708	ESO 103-G35	2	3983	43.57	—	—	—	
721	NGC 7212	2	7984	44.27	18.1	22.39	361	interacting

In the cases where the radio emission was not extended we assumed an upper limit of  $0.1''$ . These cases are indicated by a letter “u” in the last column.

TABLE 2. Measurements for galaxies with extended radio emission in the  $60\mu\text{m}$  sample

Name	Type	$PA_{MA}$	i	$PA_{RAD}$	closer side	source side	Radio Morphology	references/ comments
MRK 348	2	170	16	-15	e	rot	L	1, 9
TOL 0109-38	2	61	64	96	s	dust	S	2, 5
MRK 359	1	8	34	75	-	-	S	2, 5
MRK 573	2	5	30	125	n	rot	L	3, 5
NGC 1068	2	115	28	0	s	rot	L	4, 10
UGC 2514	1	-40	55	56	sw	dust	L	5, 5
IRAS 03106-0254	2	-14	71	37	-	-	L	5, 5
IRAS 04502-0317	2	15	59	22	e	dust	L	5, 5
IRAS 04507+0358	2	46	36	153	-	-	S	5, 5
MRK 3	2	28	33	86	-	-	L	3, 5
MRK 6	1	-46	54	-3	ne	dust	L	5, 5
MRK 79	1	-47	36	11	e	rot	L	5, 5
MRK 622	2	-35	26	0	-	-	S	2, 5
MGC-01-24-012	2	42	54	89	nw	rot	L	5, 5
NGC 3393	2	41	30	56	nw	rot	L	5, 5
NGC 3516	1	56	36	10	n	dust	L	2, 5
IRAS 11215-2806	2	-34	70	75	-	-	L	5, 5
MGC-05-27-013	2	-82	69	2	s	dust	L	5, 5
MRK 766	1	67	31	32	-	-	S	2, 5
NGC 4388	2	-89	70	21	n	dust	L	2, 5
MGC-04-31-030	2	58	62	84	n	dust	L	5, 5
MGC-03-34-064	2	48	46	39	-	-	L	5, 5
ESO 383-g18	2	88	63	178	-	-	S	5, 5
IRAS 14082+1347	2	-85	47	99	n	dust	S	5, 5
NGC 5506	2	-89	76	70	s	dust	L	5, 5
IRAS 14317-3237	2	3	41	169	-	-	L	5, 5
UGC 9944	2	-7	71	67	w	rot	L	5, 5
PKS 2048-57	2	-60	32	-65	sw	dust	L	6, 5
AKN 564	1	-73	37	6	-	-	L	5, 5
NGC 7674	2	-26	43	117	sw	rot	L	7, 5
NGC 1386	2	25	68	170	nw	dust	S	2, 5
MGC +8-11-11	1	33	16	128	-	-	L	5, 11
NGC 4941	2	17	61	-25	e	rot	L	5, 5
MRK 176	2	59	70	92	-	-	S	5, 5 interact
NGC 5548	1	-80	33	168	-	-	L	2, 5 interact
NGC 7212	2	-	-	-7	-	-	L	8, - interact

Column 7 indicates the kind of measurement used to determine the closer side of the galaxy: dust lane (dust) or rotation curve (rot). Column 8 shows the morphology of the extended radio emission, L (linear), S (slightly resolved), D (diffuse). Column 9 shows the references from which we obtained the values of  $PA_{RAD}$  and  $PA_{MA}$ , respectively. The galaxies MRK 176, NGC 5548 and NGC 7212 are show in this table because they have extended radio emission, but they are not used in the analysis, because they are interacting systems. Sources of radio data ( $PA_{RAD}$ ): (1) Ulvestad et al. (1999); (2) Nagar et al. (1999); (3) Ulvestad & Wilson (1984)b; (4) Gallimore, Baum & O’Dea (1996); (5) our measurements; (6) Morganti et al. (1999); (7) Kukula et al. (1995); (8) Falcke, Wilson & Sipmson (1998); Sources of optical data ( $PA_{MA}$ , i): (9) Simkin et al. (1987); (10) Brinks & Mundell (1996); (11) Canzian (1998).

TABLE 3. Measurements for galaxies in the serendipitous sample

Name	Type	$PA_{MA}$	ellipticity	$PA_{RAD}$	closer side	source side	Radio Morphology	references
ngc513	2	69	55	167	-	-	S+D	1,13
ngc591	2	5	33	-28	-	-	S	2,13
mrk1066	2	90	54	134	sw	dust	L	2,15
ngc1365	1	42	45	125	nw	rot	S	3,16
mrk618	1	80	39	146	s	rot	S	4,13
eso362-g8	2	-15	63	165	-	-	L	1,14
ngc2110	2	161	42	10	w	rot	L	1,17
ngc2273	2	62	50	96	-	-	L	1,14
eso428-g14	2	-44	49	129	ne	rot	L	2,14
mrk78	2	84	56	90	-	-	L	5,14
ngc2622	2	52	48	155	-	-	S	6,14
ngc2639	2	-43	53	100	ne	dust	L	7,14
ngc3227	1	158	54	173	e	rot	S	8,18
mrk34	2	65	30	158	-	-	L	5,14
ngc4051	1	132	39	81	sw	rot	L+D	5,19
ngc4117	2	18	60	177	e	dust	L	1,15
ngc4151	1	26	21	77	e	rot	L	8,20
eso323-g77	1	155	60	35	ne	dust	L	1,15
ngc5135	2	15	34	25	w	rot	A	7,14
ngc5252	2	15	59	-10	-	-	L	8,14
mrk268	2	-67	54	70	-	-	S	5,14
mrk270	2	-60	30	48	s	dust	L	5,14
ngc5273	1	11	32	5	w	dust	S	1,14
ic4329a	1	44	58	97	se	dust	L	1,14
mrk279	1	33	57	90	-	-	S	4,14
ngc5643	2	136	23	87	sw	rot	L	9,9
ngc5728	2	2	51	127	e	rot	L	10,10
mrk509	1	75	35	110	-	-	S	4,13
ngc7172	2	100	56	90	n	dust	S	11,15
ic5169	2	24	72	16	-	-	L	1,13
ngc7450	1	25	47	100	-	-	L	5,14
ngc7465	2	-19	44	32	-	-	S	1,13
mrk926	1	-88	38	90	-	-	S	4,13
ngc7672	2	28	39	95	-	-	L	7,14
ngc7743	2	86	38	21	-	-	S	1,13
eso137-g34	2	-48	40	-60	-	-	S	12,13

Column 7 indicates the kind of measurement used to determine the closer side of the galaxy: dust lane (dust) or rotation curve (rot). Column 8 shows the morphology of the extended radio emission, L (linear), S (slightly resolved), D (diffuse) and A (amorphous). Column 9 gives the references from which we obtained  $PA_{RAD}$  and  $PA_{MA}$ , respectively. Sources of  $PA_{RAD}$ : (1) Nagar et al. 1999; (2) Bower et al. 1995; (3) Sandqvist, Joersaeter & Lindblad 1995; (4) Ulvestad & Wilson 1984a; (5) Ulvestad & Wilson 1984b; (6) Ulvestad 1986; (7) Ulvestad & Wilson 1989; (8) Kukula et al. 1995; (9) Morris et al. 1985; (10) Schommer et al. 1988; (11) Unger et al. 1987; (12) Morganti et al. 1999; Sources of  $PA_{MA}$ : (13) Our measurements on DSS images; (14) Our measurements on our images; (15) RC3; (16) Ondrechen & van der Hulst 1989; (17) Wilson & Baldwin 1985; (18) Mundell et al. 1995; (19) Lizst & Dickey 1995; (20) Simkin 1975.

TABLE 4. Definition of the angles used in the models

Angle	Definition	Allowed Range
$\beta$	angle between the radio jet and the galaxy disk axis	$0^\circ - 90^\circ$
$\phi$	angle between the radio jet and line of sight	$-180^\circ - 180^\circ$
$\delta$	difference between the PA of the radio jet and the PA of the galaxy major axis	$0^\circ - 90^\circ$
$i$	inclination of the galaxy relative to the line of sight	$0^\circ - 90^\circ$
$\theta$	azimuthal angle of the radio jet	$0^\circ - 360^\circ$
$\beta_{min}$	minimum value $\beta$ can have, for a given pair $(i, \delta)$	—
$\beta_1$	minimum value $\beta$ can have in the models	$< \beta_2$
$\beta_2$	maximum value $\beta$ can have in the models	$> \sup \beta_{min}^a$
$\phi_c$	maximum value of $\phi$ for a galaxy to be recognized as a Seyfert 1	—
$i_c$	maximum value of $i$ for a galaxy to be recognized as a Seyfert 1	—

<sup>a</sup> $\sup \beta_{min}$  is the largest value of  $\beta_{min}$  among the galaxies in the sample.